A Stalagmite Test of North Atlantic SST and Iberian Hydroclimate Linkages over the Last Two Glacial Cycles

Rhawn F. Denniston[a*], Amanda N. Houts[a1], Yemane Asmerom[b], Alan D. Wanamaker, Jr.[c], Jonathon A. Haws[d], Victor J. Polyak[b], Diana L. Thatcher[c], Setsen Altan-Ochir[a], Alyssa C. Borowske[a2], Sebastian F.M. Breitenbach[e], Caroline C. Ummenhofer[f], Frederico T. Regala[g], Michael M. Benedetti[h], Nuno Bicho[i]

[a] Department of Geology, Cornell College, Mount Vernon, Iowa 52314 USA
[b] Department of Earth and Planetary Sciences, University of New Mexico, Albuquerque, New Mexico 87131 USA
[c] Department of Geological and Atmospheric Sciences, Iowa State University, Ames, Iowa 50011 USA
[d] Department of Anthropology, Louisville University, Louisville, Kentucky 40208 USA
[e] Institute for Geology, Mineralogy, and Geophysics, Ruhr-University Bochum 44801 Germany
[f] Department of Physical Oceanography, Woods Hole Oceanographic Institution, Woods Hole, Massachusetts 02543 USA
[g] Associação de Estudos Subterrâneos e Defesa do Ambiente, Torres Vedras, Portugal
[h] Department of Geography and Geology, University of North Carolina Wilmington, Wilmington, North Carolina 28403 USA
[i] Center for Archaeology and Evolution of Human Behaviour, Universidade do Algarve, Faro, Portugal

[*] corresponding author

[1] current address: Department of Earth Sciences, University of New Hampshire, Durham, New Hampshire 03824 USA

[2] current address: Department of Ecology and Evolutionary Biology, University of Connecticut, Storrs, Connecticut 06269 USA

Keywords

Iberia, hydroclimate, stalagmite, oxygen isotope, carbon isotope, $\delta^{234}U$, pollen, sea surface temperature

Abstract

Close coupling of Iberian hydroclimate and North Atlantic sea surface temperature (SST) during recent glacial periods has been identified through the analysis of marine sediment and pollen grains co-deposited on the Portuguese continental margin. While offering precisely correlatable records, these time series have lacked a directly-dated, site-specific record of continental Iberian climate spanning multiple glacial cycles as a point of comparison. Here we present a high-resolution, multi-proxy (growth dynamics and $\delta^{13}C$, $\delta^{18}O$, and $\delta^{234}U$ values) composite stalagmite record of hydroclimate from two caves in western Portugal across the majority of the last two glacial cycles (~230 ka). At orbital and millennial scales, stalagmite-based proxies for hydroclimate proxies covaried with SST, with elevated $\delta^{13}C$, $\delta^{18}O$, and $\delta^{234}U$ values and/or growth hiatuses indicating reduced effective moisture coincident with periods of lowered SST during major ice-rafted debris events, in agreement with changes in palynological reconstructions of continental climate. While in many cases the Portuguese stalagmite record can be scaled to SST, in some intervals the magnitudes of stalagmite isotopic shifts, and possibly hydroclimate, appear to have been decoupled from SST.

1. Introduction

The Portuguese continental margin is an important location for understanding variations in paleoceanographic conditions over orbital and millennial-scales (Hodell et al., 2013; Voelker and de Abreu, 2011). Here, marine sediments record basin-wide oceanographic signals while co-deposited pollen grains track coeval vegetation changes occurring across Iberia. Integrated analysis of these proxies has revealed a close coupling of North Atlantic SST, regional climate, and Iberian ecosystems during the last three glacial cycles, including changes in vegetation dynamics (Sánchez Goñi et al., 2002; Tzedakis et al., 2004; Roucoux et al., 2006; Martrat et al., 2007; Naugthon et al., 2007; Sánchez Goñi et al., 2008), atmospheric circulation (Sánchez Goñi et al., 2013), and fire frequency (Daniau et al., 2007). One commonly applied palynological metric is the abundance of temperate tree pollen, which rises during warm and wet conditions associated both with interglacials and Greenland interstadials, concomitant with shifts in Iberian margin SST (Sánchez Goñi et al., 2002; Tzedakis et al., 2004; Combourieu-Nebout et al., 2009; Fletcher et al., 2010; Chabaud et al., 2014). However, the nature of such land-sea connections is partially obscured by the size of catchments from which the pollen are derived, with some

reaching into central Iberia and spanning a range of environmental settings subject to varying climatic influences (Martin-Vide and Lopez-Bustins, 2006; Naughton et al., 2007) (Fig. 1).

Testing the links between terrestrial and marine systems benefits from continental climate archives that provide precisely-dated and high resolution rainfall-sensitive time series spanning tens of millennia, but such records remain rare in Iberia, particularly near the west Iberian margin (Fletcher et al., 2010; Moreno et al., 2012; Stoll et al., 2013). Here we present a composite stalagmite record of four proxies for hydroclimate – growth dynamics and $\delta^{13}C$, $\delta^{18}O$, and $\delta^{234}U$ values – spanning the majority of the last and penultimate glacial cycles (~230 ka) at two cave sites in western Portugal. These time series offer a rare, site-specific continental record capable of examining the coherence of SST controls on Iberian climate and ecosystem dynamics across glacial and interglacial periods. The new record provides a continental perspective of hydroclimate dynamics linked to regional oceanographic conditions.

2. Samples and Regional Setting

2.1 Environmental Setting

We report the analysis of five stalagmites (BG41, BG66, BG67, BG611, BG6LR) from Buraca Gloriosa (BG; 39º32'N, 08º47'W; 420 m a.s.l.) and one stalagmite (GCL6) from Gruta do Casal da Lebre (GCL; 39˚18'N, 9˚16'W; 130 m a.s.l.), two caves in western Portugal (Fig. 1). Environmental conditions in BG and GCL are well suited for speleothem paleoclimate reconstruction (see below). BG and GCL are located within the Meso-Mediterranean bioclimatic zone that dominates much of Iberia (Fig. 1). This region is characterized by strong seasonality, with warm, dry summers and cool, wet winters (Fig. 2) associated with the winter westerlies (Blanco Castro et al., 1997). In contrast, the Atlantic zone, north of the Douro River, is cooler, wetter, and less strongly seasonal. In the Pleistocene, the transition between these zones likely shifted southward with Mediterranean-type vegetation restricted to refugia (Rey Benayas and Scheiner, 2002).

Over interannual scales, the hydroclimate of Iberia is tightly coupled with the winter North Atlantic Oscillation (NAO) (Fig. 3), an atmospheric dipole that strongly influences precipitation across much of western Europe and that more broadly reflects the strength and positioning of the Azores high pressure system, which steers storm tracks contained within the westerlies into or north of Iberia (e.g., Trigo et al, 2002; Paredes et al., 2006; Trouet et al., 2009;

97 Cortesi et al., 2014). The NAO is typically measured as the NAO index, which is calculated
98 using atmospheric pressure differences between Iceland and Lisbon (or the Azores) (Barnston
99 and Livezey, 1987). The nature of the influence of the NAO varies across Iberia, but it is
100 strongly correlated to rainfall in western Portugal (Fig. 3), with a positive NAO index associated
101 with a steeper pressure gradient and elevated Iberian aridity. Iberian precipitation has also been
102 linked to SST in regions ranging from the western North Atlantic to the Iberian margin (Lorenzo
103 et al., 2010) where ocean circulation is dominated by the southward-flowing Portugal Current
104 and the near-coastal, north-flowing Iberian Poleward Current, two systems that transport pollen
105 from river mouths along the continental shelf (Fig. 1).
106
107 *2.2 Cave Settings*
108 Buraca Gloriosa cave is located near the town of Alvados, 30 km from the Atlantic
109 Ocean, within middle Jurassic limestones of the Estremadura Limestone Massif (Rodrigues and
110 Fonseca, 2010), a topographically distinct region in central Portugal (Fig. 1). The ~35 m-long
111 cave is accessed through a single, small (~0.5 m^2) entrance at the top of a collapse at the base of
112 a 30 m-high escarpment (Fig. 4). The cave is well decorated although little active growth is
113 occurring today. Vegetation above the cave is primarily shrubs, small trees, and mosses, hosted
114 by a thin (0-10 cm) and highly organic soil layer.
115 Gruta do Casal da Lebre overlooks the coastal town of Peniche and is hosted by upper
116 Jurassic limestones. The cave is 130 m long and contains a single, one m^2 entrance that opens
117 onto a 7 m vertical shaft (Fig. 4). This entrance has been closed with a solid metal door in recent
118 decades in order limit access to the cave, and this modification likely has reduced air exchange in
119 GCL relative to its original state. Like BG, GCL hosts little active calcite deposition, but
120 contains numerous fossil stalagmites and stalactites. The vegetation over the cave has been
121 replaced in recent decades by stands of eucalyptus that grow in thin (<1-5 cm), clay-rich soils.
122
123 *2.3 Pollen Sources*
124 Pollen deposited on the west Iberian margin is sourced primarily from vegetation
125 inhabiting the watersheds of the major west-flowing stream systems draining Portugal and Spain,
126 which are (from north to south) the Douro, Tagus, and Sado rivers. The areas encompassed by
127 these streams are large (79,000, 81,000, and 7,650 km^2, respectively) and span a variety of

elevations. The Tagus and Sado are primarily responsible for pollen deposited southwest of Portugal, while the Douro plays an important role in delivering pollen to the more northwesterly sites (Fig. 1). Prevailing wind patterns likely prevent substantial transport of pollen from Iberia to the western Portuguese margin (Naughton et al., 2007). The pollen data presented here were collected in three closely spaced cores from the southwest Iberian margin (MD01-2443: 250-194 ka (Roucoux et al, 2006; Tzedakis et al., 2004); MD01-2444: 193-136 ka (Margari et al., 2010; Margari et al., 2014); MD95-2042: 141-1 ka (Sánchez Goñi et al., 2008; Sánchez Goñi et al., 2013) (Fig. 1) and are integrated here into a single time series.

3. Materials and Methods

3.1 Environmental Monitoring

Environmental conditions were measured at both cave sites over a multi-year period, with data recorded in two-hour intervals near the areas where the stalagmites were deposited. Temperature and relative humidity were obtained using HOBO U23 automated sensors while barometric pressure was recorded with HOBO U20L loggers. Drip rates were monitored at BG with Stalagmate acoustic drip counters (Collister and Mattey, 2008).

3.2 Uranium-Series Dating

Stalagmite chronologies were constructed with a total of 69 ^{230}Th dates obtained at the University of New Mexico (Table 1) using the methods of Asmerom et al. (2010). For dating of stalagmite carbonate, powders ranging from 100-200 mg were transferred into 30 ml Teflon beakers, weighed, dissolved in 15N nitric acid, and then spiked with a mixed ^{229}Th-^{233}U-^{236}U tracer and processed using column chemistry methods. U and Th fractions were dissolved in 5 ml of 3% nitric acid and transferred to analysis tubes for measurement on a Thermo Neptune MC-ICP-MS. U and Th solutions were aspirated into the Neptune using a Cetac Aridus II low flow desolvating nebulizer and run as static routines. All isotopes of interest were measured in Faraday cups, except for ^{234}U and ^{230}Th, which were measured in the secondary electron multiplier (SEM). Gains between the SEM and the Faraday cups were determined using standard solutions of NBL-112 for U and an in-house ^{230}Th-^{229}Th standard for Th that was measured after every fifth sample; chemistry blanks reveal U and Th blanks below 20 pg. Ages are reported using two standard deviation errors.

For BG stalagmites, corrections were made for unsupported ^{230}Th using a $^{230}Th/^{232}Th$ ratio of 13.5 ppm (±50%), a value determined from isotopic analysis of cave dripwater. To obtain this value, 108 ml of dripwater were transferred into six 30 ml Teflon beakers. These beakers were fluxed in 6N HCl for an hour, rinsed, and heated gently on a hotplate until approximately 1-2 ml of fluid remained in each. All solutions were then combined into a single 30 ml Teflon beaker, spiked with the same tracer described above (which contains HF), fluxed, and then taken to complete dryness. The resulting precipitate was dissolved with 15N HNO_3, dried down, dissolved again in 7N HNO_3, and processed with the same column chemistry methods used for the stalagmite samples. We lack independent constraints on the initial Th ratio for the GCL stalagmite, and thus apply the default value of 4.4 ppm (±50%). This difference in the initial Th ratio impacts the corrected ages of GCL6 by 0.5-3.0 kyr relative to the value used for BG, and thus does not meaningfully influence our interpretations.

Age models were developed via multiple polynomial interpolations between dated intervals using the COPRA age modeling software (Breitenbach et al., 2012) (Fig. 5). Aside from providing age models, COPRA also yields mean modeled stable isotope values and confidence intervals (Supp. Fig. S1). Here we rely primarily here on the original $\delta^{18}O$ and $\delta^{13}C$ values because COPRA-derived median values reflect statistically robust variations, but reduce to some degree the range of isotopic variability. For COPRA, a dummy age was included in the age model for BG41 in order to extrapolate below the hiatus, which is only possible with at least two dated points. The value of this dummy age was based on the assumption that it maintains a stratigraphically correct slope (i.e. higher sections of the stalagmite represent younger material). The dummy age was applied a conservative error, meaning that it was as large as possible without causing stratigraphic inversion with respect to the bounding ages.

3.3 Stable Isotope Ratios

A total of 1,510 stable isotope analyses were performed on calcite samples milled from the central axis of each stalagmite. After milling, powders were weighed (~200 μg) and transferred to reaction vessels that were flushed with ultra-pure helium. Samples were then digested using >100% H_3PO_4 and equilibrated overnight (~16 hours) at 34˚C before being analyzed. Isotopic ratios were measured using a GasBench II with a CombiPal autosampler coupled to a Thermo Finnigan Delta Plus XL mass spectrometer at Iowa State University. A

combination of internal and external standards was run after every fifth sample, as well as before and after each batch, in order to ensure reproducibility. Oxygen and carbon isotope ratios are presented in parts per mil (‰) relative to the Vienna Pee Dee Belemnite carbonate standard (VPDB). Average precision for both $\delta^{13}C$ and $\delta^{18}O$ analyses is better than ±0.1‰ (1σ).

For isotopic analyses of soil organic matter and vegetation collected from above the caves, samples were dried, crushed, and transferred to tin boats. Carbon isotopic ratios were measured using a Thermo Finnegan Delta Plus XL mass spectrometer in continuous flow mode coupled with a Costech Elemental Analyzer. Caffeine (IAEA-600), cellulose (IAEA-CH-3), and acetanilide (laboratory standard) isotopic standards yielded an average analytical uncertainty for carbon of ±0.09‰ 1σ (VPDB). Dripwater samples were measured using a Picarro L2130-i Isotopic Liquid Water Analyzer, with autosampler and ChemCorrect software. Each sample was measured six times, with only the last three injections used to determine isotopic values in order to minimize memory effects. Three reference standards (VSMOW, IAEA-OH-2, IAEA-OH-3) were used for regression-based isotopic corrections and to assign the data to the appropriate isotopic scale. Reference standards were measured at least once every five samples. The average analytical uncertainty for $\delta^{18}O$ measurements was ± 0.1‰ 1σ (VSMOW).

3.4 Stalagmite Mineralogy and Fabrics

The calcite comprising the BG samples ranges across a variety of fabrics including a faster-growing, white, fibrous form and a slower-growing, dense, clear structure (Fig. 6; Supp. Fig. S2). In samples, sharp changes between the two forms within the same growth horizons mark intervals of recrystallization during which U/Th ages are highly inconsistent, and these intervals were excluded from our data set. BG6LR, which grew discontinuously over much of the last glacial cycle, suffered from alteration of early and middle Holocene material, which was therefore excluded from this analysis. BG67 is characterized primarily by fibrous calcite that has been recrystallized to clear, dense calcite in a narrow band descending through its core. U/Th dates from the fibrous calcite on the margins of the growth surface reveal open system behavior and thus this portion of BG67 was excluded. Recrystallization is evident in portions of GCL6 (particularly just above its base) and BG66 but the consistency of U/Th dates and the trends in stable isotopes suggest that this alteration may have occurred soon after original deposition. We tested whether these altered sections retain reliable paleoclimatic information by analyzing stable

isotopes along partial transects located just outside the zones of recrystallization (Fig. 6). Because stable isotopic values and trends between these transects were consistent (within the analytical errors), we retained these sections in the time series. Growth position changed at numerous times in several of these stalagmites, and our sampling strategy accounted for these changes so as to consistently collect samples for stable isotopic analysis from the top surface (cap) of each stalagmite rather than the margins.

4. Results

4.1 Environmental Monitoring

Temperature and relative humidity collected inside both caves document environmental conditions over a multi-year period. Relative humidity remained largely stable at ~100% in both caves. Temperatures, while different at the two sites, exhibited similar seasonal variability that approximates the mean average temperature of the region (14.2±0.4˚C at BG and 16.2±0.3˚C at GCL for August 2012-January 2018) (Fig. 7).

Dripwater was collected at BG both over the course of minutes during site visits on four separate occasions (November 2014, October 2015, March 2016, January 2018) and as months-long integrated samples. A total of 25 dripwater samples were analyzed for stable isotopic values. Dripwater $\delta^{18}O$ values range from -2.4‰ to -4.6‰, with a mean of -3.8±0.8‰ (Supp Table 1), although as the timing of site visits varied, this value clearly is impacted by seasonal controls on precipitation (and thus infiltration) oxygen isotope values. Drip rates were measured for much of the period spanning June 2014 to January 2018 (for a total of ~36 months) and exhibit seasonal variations tied to the winter wet and summer dry seasons, as well as individual rain events (Fig. 7).

4.2 U-Th Dates and Age Models

^{234}U-^{230}Th dating of BG and GCL stalagmites reveals growth across approximately three quarters of the last 230 ka, with periods of deposition interrupted by numerous hiatuses of varying length, with the longest gaps from 160-147, 97-87, 72-60, 41-36, 32-30, and 17-15 ka (Fig. 5 and 6; Supp. Fig. S3). These features, coupled with repeated changes in growth direction and high ^{232}Th abundances in select sections, complicate construction of a chronology in some intervals. Macroscopic petrographic discontinuities suggest the presence of several short-lived

hiatuses, but these were included as gaps in the age models only where U/Th dates reveal an identifiable temporal offset. For example, the marine isotope stage (MIS) 6/5e boundary recorded by stalagmite BG67 is marked by both a change in drip position and a sharp transition from dense, clear calcite to a white, fibrous form. Taken together, it is clear that a hiatus of some duration occurred at this time. However, these isotope data are presented as being uninterrupted given the continuity of $\delta^{18}O$ values and no U/Th evidence for a long-lived hiatus (Fig. 6).

4.3 Assessing Environmental Signals in Speleothem Isotopic Ratios

We used two approaches to assess the fidelity of BG/GCL carbon and oxygen isotopes as records of past environmental variability. First, Hendy Tests, in which stalagmite isotopic ratios must satisfy two criteria in order to be considered as having crystallized near isotopic equilibrium with cave dripwater (Hendy, 1971), were performed for each stalagmite. The first half of the Hendy Test involves analysis of multiple isotopic analyses performed on samples drilled at increasing distance from the central growth axis along the same series of growth layers. The conceptual justification for this approach is that dripwater, and thus speleothem calcite, $\delta^{18}O$ values should remain constant down the stalagmite flanks because ^{16}O preferentially lost to CO_2 out-gassing is replenished by CO_2 hydration and hydroxylation reactions. Progressive ^{18}O enrichment associated with kinetic effects tied to Rayleigh distillation suggests isotopic disequilibrium. No such consistent trends toward elevated oxygen isotopic ratios are found (Fig. 8), and thus the BG/GCL stalagmites appear to satisfy the first criterion of the Hendy Test.

The second portion of the Hendy Test is based on the degree of covariation of carbon and oxygen isotopic ratios. Oxygen isotopic ratios of speleothem calcite reflect those of infiltrating fluids, which are generally close to the $\delta^{18}O$ values of meteoric precipitation, and which, in many locations, are linked to climate (air temperature, moisture source, seasonality of precipitation, or rainfall amount). Oxygen isotopic ratios in stalagmites primarily reflect the $\delta^{18}O$ value of effective precipitation, as only an extremely small proportion of oxygen in dripwater is contributed by dissolution of CO_2 or bedrock carbonate (Lachniet, 2009). Interpreting changes in oxygen isotope composition at BG/GCL during intervals of profound climatic change such as marked the last glacial period is complicated by the multiple factors that influenced $\delta^{18}O$ values of precipitation at these sites, including shifts in moisture source. The potential exists for rainfall in Iberia to be derived from atmospheric moisture sources that change on synoptic/seasonal

scales (Moreno et al., 2014; Gimeno et al., 2010; Gimeno et al., 2012) as well as in response to changing glacial boundary conditions (Florineth and Schlüchter, 2000; Kuhlemann et al., 2008; Luetscher et al., 2016). In addition, strong but opposite correlations exist in modern precipitation between rainwater $\delta^{18}O$ values and (i) the regional air temperature (r=+0.8) and (ii) rainfall amount (r=-0.8), both of which are related to the strong seasonality of precipitation associated with Meso-Mediterranean climates (IPMA, 2016).

Stalagmite $\delta^{13}C$ values reflect two primary inputs: CO_2 derived from the atmosphere and/or soil zone and bicarbonate derived from dissolution of bedrock carbonate. Speleothem $\delta^{13}C$ values reflect the type (C_3 vs C_4) and density of vegetation over the cave, both of which are impacted by changes in air temperature and/or precipitation. The average $\delta^{13}C$ value of biogenic CO_2 in the soil zone is tied to the ratio of plants utilizing the C_3 (average $\delta^{13}C$ -26‰) versus C_4 (average $\delta^{13}C$ -14‰) photosynthetic pathways (Deines, 1980; von Fischer et al., 2008). Similarly, vegetation density and soil respiration rates over the cave impact the relative contribution of atmospheric CO_2 (pre-Industrial $\delta^{13}C$ -6‰ to -7‰; Francey et al., 1999) as compared to soil-derived CO_2 (Hellstrom and McCulloch, 2000; Genty et al., 2003). Phanerozoic bedrock $\delta^{13}C$ values range from -4‰ to +8‰ (Saltzman and Thomas, 2012), but these values are static and do not contribute to temporal variability in stalagmite carbon isotopic ratios.

Superimposed on these inputs are secondary effects capable of influencing the $\delta^{13}C$ values of dripwater in the epikarst or cave. When voids in the bedrock are not fully saturated, CO_2 degassing from infiltrated water may occur in the epikarst. This preferential loss of $^{12}CO_2$ (that may result in crystallization of calcium carbonate – so-called prior calcite precipitation) enriches the residual solution in ^{13}C, a signal that can be transferred into underlying stalagmites (Baker et al., 1997). Once the solution enters the cave, equilibrium fractionation between dissolved carbon species may be disrupted owing to issues surrounding CO_2-degassing under low drip rate conditions (Breitenbach et al., 2015) or by disequilibrium processes occurring during carbonate crystallization (Mickler et al., 2004; Fairchild et al., 2006). Importantly, $\delta^{13}C$ values reflect local infiltration rather than (pan-)regional atmospheric conditions as in the case of $\delta^{18}O$. This difference between both proxies offers the opportunity to investigate environmental changes at different spatial scales.

Correlations between carbon and oxygen isotope ratios are presented in Figure 8. Three stalagmites – BG6LR, BG66, and BG67 – show strong correlations between $\delta^{13}C$ and $\delta^{18}O$ (r^2=0.6), while the other three samples lack a strong correlation. If one considers the second criterion of the Hendy Test, the nature of equilibrium crystallization in stalagmites BG6LR, BG66, and BG67 would be considered suspect. It must be noted, however, that the reliability of the Hendy Test has been questioned because (1) equilibrium may be maintained in some portions of a stalagmite but not others, (2) growth layers thin progressively down the sides of the stalagmite, making it difficult to restrict samples to the same material, and (3) equilibrium covariation of carbon and oxygen isotope ratios may result as the direct or indirect result of climatic variability (Dorale and Liu, 2009; Lechleitner et al., 2017). We therefore interpret both isotope ratios and their covariation as environmental signals.

An additional test of equilibrium crystallization in the modern system can be constructed by comparing modeled stalagmite isotopic values to recently deposited calcite. The carbon isotopic composition of speleothem calcite is the result of a complex series of reactions that have been addressed in a number of studies (Hendy, 1971; Mühlinghaus et al., 2007; Dreybodt, 2008). For $\delta^{13}C$ in BG stalagmites, we use the equations of Li et al. (2014), which factor in the two primary sources of carbon – soil CO_2 and bedrock carbonate – the proportion of carbon derived from each source, and temperature-induced fractionation of carbon isotopes between dissolved carbon species:

$$\delta^{13}C_{calcite} = f_l * [\delta^{13}C_{ls} - (\delta^{13}C_{CO2(g)} + 9.48x10^3/T - 23.89)] + \delta^{13}C_{CO2(g)} + 9.48x10^3/T + 0.049T - 37.72$$

where: f_l = fraction of bicarbonate from limestone (ls)

T = temperature (˚K)

We assume the most straightforward and simple situation: the system remains closed to soil CO_2 and bedrock carbonate contributes 50% of carbon to dripwater bicarbonate (f_l=0.5). We apply the average cave temperature of 14.4˚C and the measured $\delta^{13}C$ values of BG bedrock and the overlying vegetation/soil of +3±1‰ and -28±1‰, respectively. This approach, while certainly overly simplified for the BG system, yields modeled stalagmite $\delta^{13}C$ values of -

342 7.7±1‰, similar to calcite crystallized on two glass slides installed at the site of two actively
343 growing stalagmites in the loft area of BG, which yielded $\delta^{13}C$ values of -8.4±1.2‰.
344 Oxygen isotopic ratios were modeled using the paleotemperature equation of Kim and
345 O'Neil (1997), which requires measurements of cave temperature and dripwater $\delta^{18}O$ values.
346 The modeled $\delta^{18}O$ value of -3.1±1.0‰ is nearly identical to the glass plate-grown calcite value
347 of -3.0±0.6‰. It should be noted, however, that assessing equilibrium crystallization in modern
348 calcite/dripwater pairs at BG is complicated by the low temporal resolution associated with
349 integrated, months-long dripwater samples, variable timing of dripwater collecting trips, and any
350 seasonal biases in calcite crystallization that at present remain poorly constrained.
351 Replication between stalagmites of similar age is arguably the single most reliable
352 method for evaluating the impacts of climate versus secondary influences, including evaporation
353 and kinetic effects (Denniston et al., 1999; Mickler et al., 2004), on stalagmite isotopic ratios
354 (Dorale and Liu, 2009; Denniston et al., 2013). When presented as an integrated data set, the
355 BG/GCL stalagmite carbon and oxygen isotopic time series spans the majority of the last 230 ka
356 (Fig. 9), although stalagmites spanning the same periods of time are restricted to 187-185, 111-
357 104, 83-81, 78-73, and 58-53 ka. Because these intervals are short, and because the temporal
358 resolution varies substantially between stalagmites, replication tests based on these intervals are
359 of limited utility. However, within the age uncertainties, $\delta^{18}O$ and $\delta^{13}C$ values and trends are
360 similar, suggesting that oxygen and carbon isotopic ratios track environmental, rather than drip-
361 specific, variables. The three exceptions in which coeval samples do not replicate well are: $\delta^{13}C$
362 values offset by 3‰ from 83-81 ka and by 4‰ from 58-53 ka, and $\delta^{18}O$ values offset by 1‰
363 from 111-104 ka (Fig. 9; Supp. Fig. S4).
364
365 *4.4 Hydroclimate Proxies*
366 *4.4.1 Carbon Isotopes*
367 Interpreting speleothem $\delta^{13}C$ variability in a climatic context requires understanding, or
368 at least constraining, the origins of these isotopic shifts. Terrestrial deposits preserving pollen
369 spectra spanning substantial portions of the last glacial cycle from western Iberia are rare
370 (Gómez-Orellana et al., 2008; Fletcher et al., 2010; Moreno et al., 2012), and thus pollen in
371 marine sediments represents a particularly important continental climate record. Pollen samples
372 obtained from the Iberian margin contain small percentages of *Poaceae*, the family including the

majority of C_4 plants, demonstrating a persistent and overwhelming majority of C_3 (largely shrub and arboreal) vegetation throughout the last glacial cycle including between Greenland stadials (GS) and interstadials (GI) and across Heinrich stadials (HS) (d'Errico and Sánchez Goñi, 2003; Tzedakis et al., 2004; Desprat et al., 2006; Sánchez Goñi et al., 2008; Sánchez Goñi et al., 2013; Margari et al., 2014). In the absence of changes in vegetation type, shifts in the source of carbon found in cave dripwater therefore likely originated with the density of vegetation and/or soil respiration rates (Genty et al., 2003). Reductions in these values are generally associated with decreases in temperature and/or increases in aridity, such as have been inferred from Iberian pollen spectra to have characterized Iberia during GS, HS, and glacial maxima (Sánchez Goñi et al., 2008; Margari et al., 2014). Complementing these effects are increases in the contribution of bedrock carbon, as well as prior calcite precipitation, reflecting a combination of longer residence times of infiltrating solutions and desaturation of voids in the epikarst above the cave, both of which are consistent with more arid climates (Baker et al., 1997; Genty et al., 2003). Thus, we interpret the carbon isotopic values of the BG/GCL record as primarily a local (hydro)climate proxy, with higher $\delta^{13}C$ values indicative of a cooler, drier climate. Integrating the GCL6 $\delta^{13}C$ record into the BG time series is complicated by the slightly different bedrock $\delta^{13}C$ values of the host rocks (Supp. Table 1) and what may have been distinct vegetation types and cave hydrologies at each cave when GCL6 was being deposited (187-160 ka). However, as previously discussed, the similar $\delta^{13}C$ values during their period of overlap (187-185 ka) suggests that the two records can be consolidated.

4.4.2 Oxygen Isotopes

The origins of BG/GCL isotopic variability appear more complex for oxygen than for carbon. Like $\delta^{13}C$ values, local $\delta^{18}O$ minima mark interstadials and interglacials. Analysis of modern precipitation data reveals equally strong, albeit inverse, correlations between precipitation $\delta^{18}O$ and both amount (r=-0.8) and air temperature (r=+0.8) effects, likely owing to the dominance of cool season precipitation in annual water budgets (IAEA/WMO, 2016) (Fig. 2). Based on these relationships, it remains possible that changes in air temperature, overall precipitation, and/or precipitation seasonality could impact the $\delta^{18}O$ values of effective moisture. That air temperature is likely not a prominent driver of stalagmite oxygen isotopic variability is supported by two observations, however. First, the slopes of the air temperature/$\delta^{18}O$

404 relationships (‰/˚C) at the three GNIP stations located closest to BG and GCL (Porto, Vila Real,
405 and Portalegre) are nearly identical (average for the three sites of 0.25±0.03‰/˚C), but opposite
406 in sign, to the calcite-water temperature dependence of oxygen isotopic fractionation (-0.2‰/˚C)
407 (Kim and O'Neil, 1997). In the simplest sense, therefore, a 1˚C increase in mean annual air
408 temperature (and thus also cave temperature) would increase precipitation $\delta^{18}O$ values by
409 approximately the same amount that the water temperature effect would lower stalagmite calcite
410 $\delta^{18}O$ values. In this simplified scenario, the net effect is a stalagmite record that is negligibly
411 influenced by multi-decadal/centennial-scale temperature changes alone. Secondly, the observed
412 shift toward lower stalagmite $\delta^{18}O$ values during interstadials and interglacials, periods of
413 elevated mean annual temperature, demonstrates that the observed positive correlation between
414 precipitation $\delta^{18}O$ and air temperature is not a dominant feature over millennial time scales. For
415 example, the 3.5‰ decrease in $\delta^{18}O$ values between MIS 6 and MIS 5e (136-128 ka) (Fig. 9) can
416 be only partially accounted for by the ~1‰ ice volume-related decrease in North Atlantic surface
417 water $\delta^{18}O$ values (Schrag et al., 1996). Other factors such as kinetics associated with humidity
418 and wind speed at the point of evaporation (Grootes et al., 1993), temperature and source of
419 atmospheric moisture (Herbert et al., 2001), and cloud evolutionary pathways (Rozanski and
420 Araguás, 1995) need also be considered but cannot account for the entirety of this shift. Because
421 of the narrow continental shelf in central Portugal, the LGM shoreline was located close to the
422 modern shoreline, thereby minimizing continental effects, and the magnitude of the impacts of
423 wind speed and ocean temperature do not appear sufficient to account for the observed
424 stalagmite $\delta^{18}O$ variability. Thus, the decrease in stalagmite $\delta^{18}O$ between the penultimate glacial
425 and last interglacial suggests that stalagmite oxygen isotope ratios are primarily recording (pan-
426)regional hydroclimate rather than temperature. The origin of the anomalously low $\delta^{18}O$ values
427 during GI 1 (dated here from 14.5-13.9 ka) are unclear (unfortunately no other BG or GCL
428 stalagmite also spans this interval) but reinforce this inverse relationship between mean annual
429 temperature and stalagmite oxygen isotope ratios.
430
431 *4.4.3 $\delta^{234}U$ Values*
432 $\delta^{234}U$ values (calculated as the difference between the age-corrected $^{234}U/^{238}U$ ratio of a
433 sample and the secular equilibrium $^{234}U/^{238}U$ ratio) of speleothem carbonate have also been used

as a proxy for paleoprecipitation (Hellstrom and McCulloch, 2000; Oster et al., 2012; Plagnes et al., 2002; Polyak et al., 2012; Zhou et al., 2005). ^{234}U exists in the stalagmite crystalline lattice due to incorporation from cave dripwater and through *in situ* production from decay of ^{238}U. Alpha recoil displaces ^{234}U from its lattice position, increasing its susceptibility to leaching by infiltrating waters, meaning that ^{234}U is selectively mobilized relative to ^{238}U in cave dripwater (Chabaux et al., 2003; Oster et al., 2012). The flux of infiltrating fluids is therefore tied to $\delta^{234}U$ values of dripwater, and thus stalagmite carbonate, such that decreases in effective precipitation and/or bedrock dissolution rate, both of which are tied to increased aridity, are associated with elevated speleothem $\delta^{234}U$ values (Hellstrom and McCulloch, 2000; Plagnes et al., 2002; Polyak et al., 2012).

As differences in $\delta^{234}U$ values between stalagmites may arise from distinct infiltration pathways (Zhou et al., 2005), complicating the integration of $\delta^{234}U$ values from multiple stalagmites into a single, cohesive data set, we restrict our analysis to stalagmite BG6LR, which represents the longest individual stalagmite record of the BG/GCL time series. While the number of $\delta^{234}U$ measurements is small compared to stable isotopic values, the temporal density of the former is sufficient to demonstrate the utility of $\delta^{13}C$ and $\delta^{18}O$ values as paleohydroclimate proxies (Fig. 9). Decreased precipitation/effective moisture is associated with elevated stalagmite $\delta^{13}C$, $\delta^{18}O$, and $\delta^{234}U$ values. The relationships between $\delta^{13}C$ and $\delta^{234}U$ values in all BG and GCL stalagmites are presented in Supp. Fig. S5.

5. Environmental Conditions at BG/GCL and Links to Iberian Margin SST

The previously discussed tests for isotopic equilibrium, including the reproducibility of carbon and oxygen isotope ratios between coeval BG and GCL stalagmites, support the notion that their $\delta^{13}C$ and $\delta^{18}O$ values may be integrated into cohesive time series reflecting paleohydroclimatic conditions and used to assess links between continental climate and SST (Fig. 10). Over the last several glacial cycles, oceanographic conditions along the western Iberian margin varied at millennial and orbital time scales in close correlation with Greenland air temperature and North Atlantic conditions and circulation (Roucoux et al., 2005; Daniau et al., 2007; Sánchez Goñi et al., 2008; Darfeuil et al., 2016). Abrupt changes in SST reflect a balance between southward expansion of subpolar waters and northward migration of subtropical water masses (de Abreu et al., 2003). During the particularly cold conditions characterizing HS and

GS, Iberian margin SST decreased by up to 9˚C (to as much as 13˚C below present values; de Abreu et al., 2003), with these changes helping to position the arctic or subarctic front at ~39˚N, the same latitude as BG and GCL. These cold surface waters reduced the production and transport of atmospheric moisture to Iberia (Eynaud et al., 2009; Voelker and de Abreu, 2011), and would have thereby influenced the timing of speleothem growth and carbon and oxygen isotopic values in BG and GCL stalagmites. Indeed, the composite BG/GCL record documents coherence, at both orbital and millennial scales, between Portuguese hydroclimate, vegetation, and Iberian margin SST during the last two glacial cycles (Fig. 10 and 11). In an attempt to quantify this covariance, we binned the SST and stalagmite stable isotope data into century-long intervals. The relatively short record of BG41 was not included, and model ages for stalagmites BG66 and GLC6 were increased by 4.0 kyr and 1.3 kyr, respectively, to improve correlation with the SST chronology. The resulting inverse correlation between SST and carbon and oxygen is strong ($r=-0.55$ and -0.52, respectively; $p<0.0001$) (Supp. Fig. S6).

5.1 Growth Intervals

The single most fundamental prerequisite to speleothem deposition is infiltration of surface waters, and thus the timing of stalagmite growth can reflect changes in mean hydroclimatic state. Deposition of multiple BG stalagmites was punctuated by hiatuses spanning similar time intervals (although the precise ages of the onset and/or termination of the hiatuses are distinct), a relationship that suggests links to changes in hydroclimate rather than random drip site-specific variability.

Hiatuses in some BG samples coincide with HS1, HS3, HS4, and HS6, and pollen spectra independently suggest increased aridity during HS and glacial maxima. Decreases in arboreal pollen abundance and concomitant increases in drought-tolerant vegetation coincide with periods of reduced SST. Vegetation patterns during maximal IRD deposition on the Iberian margin reveal not only dramatically reduced forest cover but also a pronounced expansion of semi-desert plants (e.g. Sánchez Goñi et al., 2000; Roucoux et al., 2005; Naughton et al., 2009). These changes mark the long hiatus between HS7 and HS6 (71-59 ka), which overlaps with the some of the coldest SST of the last 70 ka as reconstructed using $U^{k}_{37}{}'$ at core MD95-2042 (Darfeuil et al., 2016) (Fig. 10; Fig. 12). An absence in BG stalagmite deposition from ~160-149 ka occurs at the same time as massive seasonal discharges from the Fleuve Manche river and the coldest

continental climates and SST (157-154 ka) of the last 230 ka, as determined from pollen and foraminifera from core MD01-2444 (Margari et al., 2014; Fig. 1).

Whether hiatuses in BG speleothem deposition are a result of pronounced reductions in precipitation, an extension of below freezing temperatures that limited infiltration (Vaks et al., 2013; Fankhauser et al., 2016), or variations in infiltration pathway/drip position is ambiguous. Pollen transfer functions from MD95-2042 suggest winter temperatures dropped below 0˚C during HS and annual precipitation was reduced by up to 50% (from 800 mm to 500-400 mm during HS3, HS4, and HS5) (Sánchez Goñi et al., 2002). Applying this temperature reconstruction to western Portugal is complicated, however, by the broad area across which these pollen were sourced. Permafrost reconstructions (Vandenberghe et al., 2014) of Iberia argue against the hypothesis that continuous sub-zero temperatures inhibited infiltration and stalagmite growth. We thus suggest that the hiatuses observed at BG and GCL were driven largely by reductions in precipitation.

Other western European cave records also share similar growth histories. For example, stalagmites from Villars Cave, southwestern France (Genty et al., 2003; Genty et al., 2010; Wainer et al., 2011), and from multiple caves in northern Spain (Stoll et al., 2013) (Fig. 1) are also punctuated by hiatuses during HS. For example, at or near HS7, stalagmite hiatuses were formed at Villars Cave (78-76 ka), in northern Spain (~75 k), and BG (80-78 ka). No stalagmite deposition has been identified at BG from 71-60 ka or Villars cave from 67-62 ka, a period that includes HS6. Finally, HS1 is marked by a hiatus in northern Spain (18-15.5 ka) and at BG (17-15 ka). While the timing of these hiatuses is not identical, and not all hiatuses at Villars Cave and the Spanish caves are coincident with those at BG, the substantial degree of overlap suggests a common origin. Stoll et al. (2013) noted that stalagmite deposition and/or elevated growth rates in northern Spain stalagmites occurred during periods of high Northern Hemisphere summer insolation or during GI, while hiatuses occurred during periods of low insolation and low SST (<13.7˚C). The BG record supports the hypothesis that growth interruptions are related to SST controls on regional atmospheric moisture availability, although the impact of insolation is not clear.

5.2 BG/GCL Stable Isotopic and $\delta^{234}U$ Variability

Stalagmite $\delta^{13}C$ and $\delta^{18}O$ values covary with changes in SST at orbital time scales. The offset between interglacial and glacial isotopic values averages ~3‰ for $\delta^{18}O$ and ~7‰ for $\delta^{13}C$ values (Fig. 10). Stalagmite $\delta^{234}U$ values also preserve these changes in aridity. Millennial-scale changes are also recorded in stalagmite carbon isotope ratios, with shifts of 3-7‰ associated with GI/GS transitions, and oxygen isotopic changes of ~1-2‰. The large swing in $\delta^{18}O$ values during the transition from GI-1 to the Younger Dryas (YD) (~5‰ from 14.0-13.5 ka) is anomalous. Given that the change in $\delta^{13}C$ values at this time (6‰) is consistent with other GI transitions, the hydroclimatic implications of this interval require additional study. Similarly, oxygen and carbon isotopic variability is pronounced during the late Holocene portion of the BG record. The origin of this high variability is unclear. Replication of the Holocene portion of this record currently underway will help address this question (Thatcher et al., 2018).

Where growth is continuous during HS, the link between stalagmite isotopic variations and SST changes is clearly visible (Fig. 11). Prominent positive carbon isotopic excursions define the YD, HS2, HS5, HS6, and HS8, consistent with diminished concentrations of arboreal pollen in cores from the Iberian margin, and serve to document particularly cold and dry conditions at these times (Sánchez Goñi et al., 2000; Roucoux et al., 2006; Sánchez Goñi et al., 2008). Reduced stalagmite $\delta^{13}C$ values mark periods of enhanced effective moisture from 170-160 and 145-135 ka, tracking peaks in temperate tree pollen and alkenone-based SST. The BG record reveals a pronounced increase in stalagmite $\delta^{13}C$ values during the YD, at odds with the plateau in SST observed in some Portuguese coastal margin sediments at this time. However, a higher resolution SST record reveals a pronounced drop in SST (Rodrigues et al., 2010), well matched with the BG isotopic profile and the stalagmite record from Villars Cave.

Hydroclimatic shifts associated with GS and GI are most clearly expressed during MIS 5a and 5b in the BG carbon isotope record (Fig. 11). Other European stalagmite records have identified GI/GS events from the last glacial period (Genty et al., 2003; Spötl et al., 2006; Boch et al., 2011; Moseley et al., 2014) (Fig. 10), but the level of resolution recorded in the BG/GCL time series has not been clearly identified previously in western Iberia. A carbon isotope time series (albeit with low temporal resolution) of a flowstone from southeastern Spain does not present clear evidence of either GI or most HS during the last glacial cycle, although it does contain a clear expression of HS11 (Hodge et al., 2008) (Fig. 1). And while some Iberian lakes and peat bogs document environmental changes concurrent with HS, no single record, including

one of the longest - the 50 ka time series from the Fuentillejo maar, south-central Spain - contains a consistent signal for all HS (Vegas et al., 2010; Moreno et al., 2012) (Fig. 1). GS/GI oscillations during MIS 3 are not clearly defined in BG stalagmites, likely owing to insufficient temporal resolution, although the BG records does share a resemblance to reconstructed SST variability (Fig. 11).

Whether the apparent inconsistent linkages between Iberian margin SST and Iberian hydroclimate are due to the limitations of these proxies, region-specific responses to SST variations, or a changing influence of SST on precipitation is unclear. However, other points of divergence between SST and the BG/GCL records exist. For example, some marine cores reveal a prominent spike in forest taxa occurring at the start of interglacials, decreasing thereafter for the next 5-10 kyr (Tzedakis et al, 2004; Desprat et al., 2007) (Fig. 10). This early interglacial peak is a common feature in several time series including the Antarctic δD (Petit et al., 1999) and CH_4 records (Loulergue et al., 2008), and in stalagmite isotopic ratios from the eastern Mediterranean (Bar-Matthews et al., 2003) and southern France (Couchoud et al., 2009) (Fig. 10). The BG/GCL $\delta^{13}C$ and $\delta^{18}O$ records lack this feature, although the previously discussed issues surrounding the continuity of the MIS6/5e transition may complicate identifying it.

Stalagmite $\delta^{13}C$ and $\delta^{18}O$ values are lower during GI 20-22 (MIS 5a/4; 84-72 ka) than in either the Holocene or MIS 5e (Fig. 10 and 12), and BG6LR $\delta^{234}U$ values support this observation. This interval is of particular interest given that Atlantic forest pollen, which has been used as a proxy for air temperature, was decoupled from SST across northwestern Iberia during cold events (C18-C20) (Rousseau et al., 2006; Rasmussen et al., 2014). This decoupling is interpreted as reflective of a weakened control of SST on Iberian atmospheric temperature that, in turn, enhanced transport of atmospheric vapor to the high latitudes, amplifying production of ice sheets in the early stages of the last glacial cycle (Sánchez Goñi et al., 2013). This process has also been demonstrated for an earlier interglacial (MIS 19; Sánchez Goñi et al., 2016). Other offsets include (1) the gradual change in BG $\delta^{13}C$ and $\delta^{18}O$ values across the MIS 8/7 boundary, in contrast to the sharp rise in SST at this time; (2) the anomalously large $\delta^{13}C$ response to ice rafting event C24 (111-108 ka), and (3) the persistence of low $\delta^{13}C$ values as SST decreased from 205-187 ka (Fig. 11 and 12).

The mechanism linking SST and Iberian hydroclimate over millennial time scales remains unclear. The NAO exerts a strong control over Iberian precipitation, and previous

588 studies have suggested that GS and GI (Moreno et al., 2002; Sánchez Goñi et al., 2002; Daniau
589 et al., 2007) and HS (Naughton et al., 2009) were characterized by distinct NAO modes. The
590 dynamics of the NAO and Azores High pressure system prior to the historical era are only
591 beginning to be understood (Trouet et al., 2009; Olsen et al., 2012; Wassenburg et al., 2013), and
592 the BG/GCL record cannot address this question independently. However, rainfall variability in
593 eastern Iberia is less closely tied to the NAO than is western Iberia and instead reflects other
594 climatic phenomena including the El Niño-Southern Oscillation (Rodó et al., 1997), helping to
595 produce an east-west precipitation gradient. Additional high-resolution speleothem records from
596 central and eastern Iberia could therefore provide a more robust test of the underlying drivers of
597 millennial-scale hydroclimatic changes during recent glacial periods.
598
599 **6. Conclusions**
600 The BG/GCL composite speleothem record demonstrates that the hydroclimate and
601 vegetation dynamics in west-central Portugal tracked Iberian margin SST over orbital and
602 millennial scales during the past two glacial cycles. Enhanced aridity characterized HS, as
603 evidenced by elevated carbon and oxygen isotopic ratios and/or hiatuses in stalagmite growth,
604 consistent with other regional stalagmite time series. GI/GS variability expressed in the Iberian
605 margin SST record and in co-deposited pollen spectra is also present in the BG/GCL time series,
606 and is particularly well defined in MIS 5a and 5b. Understanding differences between the
607 structures of the stalagmite and SST records during some time intervals will require development
608 of speleothem records from central and southern Iberia.
609
610 **Acknowledgements**
611 This work was supported by the Center for Global and Regional Environmental Research
612 and Cornell College (to R.F.D.), and the U.S. National Science Foundation (grant BCS-1118155
613 to J.A.H., BCS-1118183 to M.M.B., and AGS-135539 to C.C.U.). Field sampling performed
614 under the auspices of IGESPAR (to J.A.H.) and Associação de Estudos Subterrâneos e Defesa do
615 Ambiente. Brandon Zinsious and Stephen Rasin contributed to fieldwork at BG, and Zachary
616 LaPointe assisted with radioisotopic analyses; Suzanne Ankerstjerne performed stable isotope
617 measurements. Use of the following data sets is gratefully acknowledged: Global Precipitation
618 Climatology Center data by the German Weather Service (DWD) accessed

through http://gpcc.dwd.de; NAO Index Data provided by the Climate Analysis Section, NCAR, Boulder, USA, Hurrell (2003). Updated regularly. Accessed through https://climatedataguide.ucar.edu/climate-data/hurrell-north-atlantic-oscillation-nao-index-pc-based. This manuscript benefitted from discussions with Maria F. Sánchez Goñi, David Hodell, and Chronis Tzedakis. We thank four anonymous reviewers, whose detailed and thoughtful assessment of the original version of this manuscript substantially improved its scope and clarity. Stable and U-series isotope data are available at the NOAA National Centers for Environmental Information website.

References

de Abreu, L., Shackleton, N.J., Schönfeld, J., Hall, M., and Chapman, M.: Millennial-scale oceanic climate variability off the Western Iberian margin during the last two glacial periods, Marine Geol, 196, 1-20, 2003.

Asmerom, Y., Polyak, V., Burns, S.: Variable winter moisture in the southwestern United States linked to rapid glacial climate shifts, Nat Geosci, 3, 114-117, 2010.

Baker, A., Ito, E., Smart, P., McEwan, R.: Elevated and variable values of ^{13}C in speleothems in a British cave system, Chem Geol, 136, 263-270, 1997.

Barker, S., Knorr, G., Edwards, R.L., Parrenin, F., Putnam, A.E., Skinner, L.C., Wolff, E., Ziegler, M.: 800,000 years of abrupt climate variability, Science, 334, 347-351, 2011.

Bar-Matthews, M., Ayalon, A., Gilmour, M., Matthews, A., Hawkesworth, C.J.: Sea-land oxygen isotopic relationships from planktonic foraminifera and speleothems in the Eastern Mediterranean region and their implication for paleo-rainfall during interglacials intervals, Geochim Cosmochim Ac, 67, 3181–3199, 2003.

Barnston, A.G. and Livezey, R.E.: Classification, seasonality, and persistence of low-frequency atmospheric circulation patterns, Mon Weather Rev, 115, 1083–1126, 1987.

Berger, A. and Loutre, M.F.: Insolation values for the climate of the last 10 million years. Quaternary Sci Rev 10, 297-318, 1991.

Blanco Castro, E., Casado González, M.A., Costa Tenorio, M., Escribano Bombín, R., García Antón, M., Génova Fuster, M., Gómez Manzaneque, F., Gómez Manzaneque, A., Moreno Sáiz, J.C., Morla Juaristi, C., Regato Pajares, P., Sáiz Ollero, H.: Los bosques ibéricos. Planeta, Barcelona, 1997.

650 Boch, R., Cheng, H., Spötl, C., Edwards, R.L., Wang, X., Hauselmann, Ph.: NALPS: a precisely
651 dated European climate record 120-60 ka, Clim Past, 7, 1049-1072, 2011.
652 Breitenbach, S.F.M., Rehfeld, K., Goswami, B., Baldini, J.U.L., Ridley, H.E., Kennett, D.J.,
653 Prufer, K.M., Aquino, V.V., Asmerom, Y., Polyak, V.J., Cheng, H., Kurths, J., Marwan, N.:
654 Constructing proxy records from age models (COPRA), Clim Past, 8, 1765-1779, 2012.
655 Breitenbach, S.F.M., Lechleitner, F.A., Meyer, H., Diengdo, G., Mattey, D., Marwan, N.: Cave
656 ventilation and rainfall signals in dripwater in a monsoonal setting – a monitoring study from
657 NE India, Chem Geol, 402, 111-124, 2015.
658 CDG: The Climate Data Guide: Hurrell North Atlantic Oscillation (NAO) Index (PC-based).
659 Retrieved from https://climatedataguide.ucar.edu/climate-data/hurrell-north-atlantic-
660 oscillation-nao-index-pc-based, accessed 21 May, 2018.
661 Chabaud, L., Sánchez Goñi, M.F., Desprat, S., Rossignol, L.: Land-sea climatic variability in the
662 eastern North Atlantic subtropical region over the last 14,200 years: Atmospheric and
663 oceanic processes at different timescales Holocene, 24, 787-797, 2014.
664 Chabaux, F., Riotte, J., Dequincey, O.: U–Th–Ra fractionations during weathering and river
665 transport. Rev Mineral Geochem, 52, 533–576. 2003.
666 Collister, C. and Mattey, D.: Controls on water drop volume at speleothem drip sites: An
667 experimental study. J Hydrol, 358, 259-267, 2008.
668 Combourieu-Nebout, N., Peyron, O., Dormoy, I., Desprat, S., Beaudouin, C., Kotthoff, U.,
669 Marret, F.: Rapid climatic variability in the west Mediterannean during the last 25 000 years
670 from high resolution pollen data, Clim Past, 5, 503-521, 2009.
671 Cortesi, N., Gonzalez-Hidalgo, J.C., Trigo, R.M., and Ramos, A.M.: Weather types and spatial
672 variability of precipitation in the Iberian Peninsula. International Journal of Climatology, 34,
673 2661-2677, 2014.
674 Couchoud, I, Genty, D., Hoffman, D., Drysdale, R., Blamart, D.: Millennial-scale climate
675 variability during the Last Interglacial recorded in a speleothem from south-western France.
676 Quaternary Sci Rev, 28, 3263-3274, 2009.
677 Daniau, A.-L., Sánchez Goñi, M.F., Beaufort, L., Laggoun-Defarge, F., Loutre, M.-F., Duprat, J.:
678 Dansgaard-Oeschger climatic variability revealed by fire emissions in southwestern Iberia.
679 Quaternary Sci Rev, 26, 1369-1383, 2007.

680 Darfeuil, S., Ménot, G., Giraud, X., Rostek, F., Tachikawa, K., Garcia, M., Bard, É.: Sea surface
681 temperature reconstructions over the last 70 kyr off Portugal: Biomarker data and regional
682 modeling, Paleocean, 31, 40–65, 2016.
683 Deines, P.: The isotopic composition of reduced organic carbon. Handbook of Environmental
684 Isotope Geochemistry, The Terrestrial Environment, Part A (Fritz, P. and Fontes, J., Eds.,
685 Elseveier, New York, 331-406, 1980.
686 Denniston, R.F., González, L.A., Asmerom, Y., Baker, R.G., Reagan, M.K. Bettis, E.A. III.:
687 Evidence for increased cool season moisture during the middle Holocene, Geology, 27, 815-
688 818, 1999.
689 Denniston, R.F., Wyrwoll, K.-H., Polyak, Brown, J. Asmerom, Y., Wanamaker, A. Jr., LaPointe,
690 Z., Ellerbroek, R., Barthelmes, M., Cleary, D., Cugley, J., Woods, D., Humphreys, W.: A
691 Stalagmite Record of Holocene Indonesian-Australian Summer Monsoon Variability from
692 the Australian Tropics. Quaternary Sci Rev 78, 155-168, 2013.
693 Desprat et al.: Climatic variability of Marine Isotope Stage 7: direct land-sea-ice correlation from
694 a multiproxy analysis of a north-western Iberian margin deep-sea core. Quaternary Sci Rev
695 25, 1010-1026, 2006.
696 Desprat, S., Sánchez Goñi, M.F., Naughton, F., Turon, J.-L., Duprat, J., Malaizé, B., Cortijo, E.,
697 Peypouquet, J.-P.: Climate variability of the last five isotopic interglacials: Direct land-sea-
698 ice correlation from the multiproxy analysis of North-Western Iberian margin deep-sea cores,
699 Editor(s): F. Sirocko, M. Claussen, M.F. Sánchez Goñi, T. Litt *In* Developments in
700 Quaternary Sciences, Elsevier, pp. 375-386, 2007.
701 Dorale, J.A., and Liu, Z.: Limitations of Hendy Test criteria in judging the paleoclimatic
702 suitability of speleothems and the need for replication. J Cave Karst Stud, 71, 73-80, 2009.
703 Dreybodt, W.: Evolution of the isotopic composition of carbon and oxygen in a calcite
704 precipitating H2O-CO2-CaCO3 solution and the related isotopic composition of calcite in
705 stalagmites. Geochim. Cosmochim. Acta, 72, 4712-4724, 2008.
706 Eynaud et al.: Position of the Polar Front along the western Iberian margin during key cold
707 episodes of the last 45 ka, Geochem Geophy Geosys, 10, Q07U05,
708 doi:10.1029/2009GC002398, 2009.

709 Fairchild, I.J., Smith, C.L., Baker, A., Fuller, L., Spötl, C., Mattey, D., McDermott, F., E.I.M.F.:
710 Modification and preservation of environmental signals in speleothems. Earth Sci Rev 75,
711 105-153, 2006.
712 Fankhauser, A., McDermott, F., and Fleitmann, D.: Episodic speleothem deposition tracks the
713 terrestrial impact of millennial-scale last glacial climate variability in SW Ireland, Quaternary
714 Sci Rev, 152, 104-117, 2016.
715 von Fischer, J.C., Tieszen, L.L., and Schimel, D.S.: Climate controls on C_3 vs. C_4 productivity in
716 North American grasslands from carbon isotope composition of soil organic matter. Global
717 Change Bio, 14, 1–15, 2008.
718 Fletcher, W.J., Sánchez Goñi, M.F., Allen, J.R.M., Cheddadi, R., Combourieu-Nebout, N.,
719 Huntley, B., Lawson, I., Londiex, L., Magri, D., Margari, v., Müller, U.C., Naughton, F.,
720 Novenko, E., Roucoux, K., Tzedakis, P.C.: Millennial scale variability during the last glacial
721 in vegetation records from Europe. Quaternary Sci Rev, 29, 2839-2864, 2010.
722 Florineth, D. and Schlüchter, S. Alpine Evidence for Atmospheric Circulation Patterns in Europe
723 during the Last Glacial Maximum. Quaternary Research, 54, 295-308, 2000.
724 Francey, R. J., Allison, C. E., Etheridge, D. M., Trudinger, C. M., Enting, I. G., Leuenberger, M.,
725 Langenfelds, R. L., Michel, E., and Steele, L. P. A.: 1000-year high precision record of ^{13}C in
726 atmospheric CO_2. Tellus B: Chemical and Physical Meteorology, 51, 170-193, 1999.
727 Genty, D., Blamart, D., Ouahdi, R., Gilmour, M., Baker, A., Jouzel, J., Van-Exter, S.: Precise
728 dating of Dansgaard-Oeschger climate oscillations in western Europe from stalagmite data,
729 Nature, 421, 833-837, 2003.
730 Genty, D., Comboruieu-Nebout, N., Peyron, O., Blamart, D., Wainer, K., Mansuri, F., Ghaleb,
731 B., Isabello, L., Dormoy, I., von Grafenstein, U., Bonelli, S., Landais, A., Brauer, A.:
732 Isotopic characterization of rapid climatic events during OIS3 and OIS4 in Villars Cave
733 stalagmites (SW-France) and correlation with Atlantic and Mediterranean pollen records.
734 Quaternary Sci. Rev., 29, 2799-2820, 2010.
735 Genty, D., Blamart, D., Ghaleb, B., Plagnes, V., Causse, Ch., Bakalowicz, M., Zouari, K., Chkir,
736 N., Hellstrom, J., Wainer, K., and Bourges, F.: Timing and dynamics of the last deglaciation
737 from European and North African $\delta^{13}C$ stalagmite profiles – comparison with Chinese and
738 South Hemisphere stalagmites. Quaternary Sci Rev 25, 2118-2142, 2006.

739 Gimeno, L., Nieto, R., Trigo, R.M., Vicente-Serrano, S.M., and López-Moreno, J.I., Where does
740 the Iberian Peninsula moisture comr from? An answer based on a Lagrangian approach. J.
741 Hydrometeorology, 11, 421-436, 2010.
742 Gimeno, L., Stohl, A., Trigo, R.M., Dominguez, F., Yoshimura, K., Yu., L., Drumond,A.,
743 Durán-Quesada, A.M., Nieto, R.: Oceanic and terrestrial sources of continental precipitation.
744 Rev Geophy, 50, 1-41, 2012.
745 Gómez-Orellana, L., Ramil-Rego, P., & Sobrino, C. M.: The Würm in NW Iberia, a pollen
746 record from Area Longa (Galicia). Quaternary Res, 67, 438-452, 2008.
747 Grootes, P. M.: *Climate Change in Continental Isotopic Records*, P. K. Swart, K. C. Lohmann, J.
748 McKenzie, S. Savin, Eds. (American Geophysical Union, Washington, DC), pp. 37- 46,
749 1993.
750 Hellstrom, J. and McCulloch, M.: Multi-proxy constraints on the climatic significance of trace
751 element records from a New Zealand speleothem. Earth Planet Sci Lett, 179, 287-297, 2000.
752 Hendy, C.: The isotopic geochemistry of speleothems – I. The calculation of the effects of
753 different modes of formation on the isotopic composition of speleothems and their
754 applicability as palaeoclimatic indicators. Geochimica et Cosmochica Acta 35, 801-824,
755 1971.
756 Herbert, T.D., Schuffert, J.D., Heusser, L., Lyle, M., Mix, A., Ravelo, A.C., Stott, L.D., and
757 Herguera, J.C.: Collapse of the California current during glacial maxima linked to climate
758 change on land. Science, 293, 71-76, 2001.
759 Hodell, D., Crowhurst, S., Skinner, L., Tzedakis, P.C., Margari, V., Channell, J.E.T., Kamenov,
760 G., Maclachlan, S., Rothwell, G.: Response of Iberian margin sediments to orbital and
761 suborbital forcing over the past 420 ka, Paleoceanography, 28, 185-199, 2013.
762 Hodge, E.J., Richards, D.A., Smart, P.L., Andreo, B., Hoffman, D.L., Mattey, D.P., Gonzales-
763 Ramon, A.: Effective precipitation in southern Spain (~266 to 46 ka) based on a speleothem
764 stable carbon isotope record. Quaternary Res, 69, 447-457, 2008.
765 IAEA/WMO: Global Network of Isotopes in Precipitation. The GNIP Database. Accessible at:
766 http://www.iaea.org/water, 2016.
767 IPMA: Accessible at http://www.meteo.pt/en/oclima/clima.normais/015/, 2012.
768 Justino, F. and Peltier, W.R.: The glacial North Atlantic Oscillation. Geophysical Research
769 Letters, 32, L21803, 2008.

770 Kim, S.-T. and O'Neil, J.R.: Equilibrium and nonequilibrium oxygen isotope effects in synthetic
771 carbonates: Geochim Cosmochim Ac, 61, 3461-3475, 1997.
772 Kuhlemann, J et al.: Regional synthesis of Mediterranean atmospheric circulation during the Last
773 Glacial Maximum. Science, 321, 1338– 1340, 2008.
774 Lachniet, M.S.: Climatic and environmental controls on speleothem oxygen isotope values.
775 Quaternary Sci Rev 28, 412-432, 2009.
776 Lechleitner, F.A., Breitenbach, S.F.M., Cheng, H., Plessen, B.: Climatic and in-cave influences
777 on d18O and d13C in a stalagmite from northeastern India through the last deglaciation. Quat
778 Res, 88, 458-471, 2017.
779 Li, Z-H., Driese, S.G., Cheng, H.: A multiple cave deposit assessment of suitability of
780 speleothem isotopes for reconstructing palaeo-vegetation and palaeo-temperature.
781 Sedimentology, 61, 749-766, 2014.
782 Lorenzo, M.N., Iglesias, I., Taboada, J.J., Gomez-Gesteira, M.: Relationship between monthly
783 rainfall in northwest Iberian Peninsula and North Atlantic sea surface temperature. Int J
784 Climatology, 30, 980-990, 2010.
785 Loulergue, L., Schilt, A., Spahni, R., Masson-Delmotte, V., Blunier, T., Lemieux, B., Barnola,
786 J.-M., Raynaud, D., Stocker, T.F., Chappellaz, J.: Orbital and millennial-scale features of
787 atmospheric CH4 over the past 800,000 years, Nature, 453, 383-386, 2008.
788 Luetscher, M., Boch, R., Sodemann, H., Spötl, C., Cheng, H., Edwards, R.L., Frisia, S., Hof, F.,
789 and Müller, W.: North Atlantic storm track changes during the Last Glacial Maximum
790 recorded by Alpine speleothems. Nature Communications, 6, DOI: 10.1038/ncomms7344,
791 2016.
792 Margari, V., Skinner, L.C., Tzedakis, P.C., Ganopolski, A., Vautravers, M., and Shackleton,
793 N.J.: The nature of millennial-scale climate variability during the past two glacial periods:
794 Nature Geoscience, v. 3, p. 127–131, doi:10.1038/ngeo740, 2010.
795 Margari, V., Skinner, L.C., Hodell, D.A., Martrat, B., Toucanne, S., Grimalt, J.O., Gibbard, P.L.,
796 Lunkka, J.P., Tzedakis, P.C.: Land-ocean changes on orbital and millennial time scales and
797 the penultimate glaciation, Geology, 42, 183-186, 2014.
798 Martin-Vide, J. and Lopez-Bustins, J-A.: The Western Mediterranean Oscillation and rainfall in
799 the Iberian Peninsula. Int J Climatol, 26, 1455-1475, 2006.

800 Martrat, B., Grimalt, J.O., Shackleton, N.J., de Abreu, L., Hutterli, M.A., Stocker, T.F.: Four
801 climate cycles of recurring deep and surface water destabilizations on the Iberian margin,
802 Science, 317, 502-507, 2007.
803 McManus, J.F., Oppo, D.W., Cullen, J.L.: A 0.5-Million-Year Record of Millennial-Scale
804 Climate Variability in the North Atlantic, Science, 283, 971-975, 1999.
805 Mickler, P.J. et al.: Stable isotope variations in modern tropical speleothems: Evaluation
806 equilibrium vs. kinetic isotope effects. Geochim Cosmochim Acta. 68, 4381-4393, 2004.
807 Moreno, A., Cacho, I., Canals, M., Prins, M.A., Sánchez Goñi, M.F., Grimalt, J.O., Weltje, G.J:
808 Saharan dust transport and high-latitude glacial climate variability: the Alboran Sea record.
809 Quaternary Res, 58, 318-328, 2002.
810 Moreno, A., Gonzalez-Samperiz, P., Morellon, M., Valero-Garces, B.L., Fletcher, W.J.:
811 Northern Iberian abrupt climate change dynamics during the last glacial cycle: a view from
812 lacustrine sediments. Quaternary Sci Rev, 36, 139-153, 2012.
813 Moreno, A., Sancho, C., Bartolumé, M., Oliva-Rucia, B., Delgado-Huertas, A., José, Estrela, M.,
814 Corell, D., López-Moreno, J.I., Cacho, I.: Climate controls on rainfall isotopes and their
815 effects on cave drip water and speleothem growth: the case of Molinos cave (Teruel, NE
816 Spain). Clim Dyn, 43, 221-241, 2014.
817 Moseley, G.E., Spötl, C., Scensson, A., Cheng, H., Brandstatter, S., Edwards, R.L.: Multi-
818 speleothem record reveals tightly coupled climate between central Europe and Greenland
819 during Marine Isotope Stage 3. Geology, 42, 1043-1946, 2014.
820 Mühlinghaus, C., Scholz, D., and Mangini, A.: Modelling stalagmite growth and d13C as a
821 function of drip interval and temperature. Geochim. Cosmochim. Acta, 71, 2780-2790, 2007.
822 Naughton, F., Sánchez Goñi, M.F., Desprat, S., Turon, J.-L., Duprat, J., Malaizé, B., Joli, C.,
823 Cortijo, E., Drago, T., Freitas, M.C.: Present-day and past (last 25,000 years) marine pollen
824 signal off western Iberia. Mar Micropaleontol, 62, 91–114, 2007.
825 Naughton, F., Sánchez Goñi, M.F., Kageyama, M., Bard, E., Duprat, J., Cortijo, E., Desprat, S.,
826 Malaizé, B., Joly, C., Rostek, F., Turon, J.-L.: Wet to dry climatic trend in north-western
827 Iberia within Heinrich events. Earth Planet Sc Lett, 284, 329-342, 2009.
828 North Greenland Ice Core Project members: High-resolution record of Northern Hemisphere
829 climate extending into the last interglacial period, Nature, 431, 147-151, 2004.

Olsen, J., Anderson, N.J., and Knudsen, M.F.: Variability of the North Atlantic Oscillation over the past 5,200 years. Nature Geoscience, 5, 808-812, 2012.

Oster, J.L., Ibarra, D.L., Harris, C.H., Maher, K.: Influence of eolian deposition and rainfall amounts on the U-isotopic composition of soil water and soil minerals. Geochim Cosmochim Ac, 88, 146 – 166, 2012.

Paredes, D., Trigo, R.M., Garcia-Herrera, R., Franco Trigo, I.: Understanding precipitation changes in Iberia in early spring: weather typing and storm-tracking approaches. J Hydrometeorol, 7, 101-113, 2006.

Petit, J.R., Jouzel, J., Raynaud, D., Barkov, N.I., Barnola, J.-M., Basile, I., Bender, M., Chappellaz, J., Davis, M., Delaygue, G., Delmotte, M., Kotlyakov, V.M., Legrand, M., Lipenkov, V.Y., Lorius, C., Pepin, L., Ritz, C., Saltzman, E., Stievenard, M.: Climate and atmospheric history of the 420,000 years from the Vostok ice core, Antarctica. Nature, 399, 429-436, 1999.

Plagnes, V., Causse, C., Genty, D., Paterne, M., Blamart, D.: A discontinuous climatic record from 187 to 74 ka from a speleothem of the Clamouse Cave (south of France). Earth Planet Sci Lett, 201, 87-103, 2002.

Polyak, V.J., Asmerom, Y., Burns, S.J., and Lachniet, M.S.: Climatic backdrop to the terminal Pleistocene extinction of North American mammals, Geology, 40, 1023-1026, 2012.

Rasmussen, S.O. et al.: A stratigraphic framework for abrupt climatic changes during the Last Glacial period based on three synchronized Greenland ice-core records: redefining and extending the INTIMATE event stratigraphy, Quaternary Sci Rev, 106, 14–28, 2014.

Rey Benayas, J.M. and Scheiner, S.M.: Plant diversity, biogeography and environment in Iberia: Patterns and possible causal factors. J Veg Sci, 13, 245-258, 2002.

Rodó, X., Baert, E., Comin, F.A.: Variations in seasonal rainfall in Southern Europe during the present century: relationships with the North Atlantic Oscillation and the El Niño-Southern Oscillation. Clim Dynam, 13, 275-284, 1997.

Rodrigues et al.: The last glacial-interglacial transition (LGIT) in the western mid-latitudes of the North Atlantic: Abrupt sea surface temperature change and sea level implications. Quaternary Sci Rev, 29, 1853-1862, 2010.

Roucoux, K.H., de Abreu, L., Shackleton, N.J., Tzedakis, P.C.: The response of NW Iberian vegetation to North Atlantic climate oscillations during the last 65kyr, Quaternary Sci Rev, 24, 1637-1653, 2005.

Roucoux, K.H., Tzedakis, P.C., de Abreu, L., Shackleton, N.J.: Climate and vegetation changes 180,000 to 345,000 years ago recorded in a deep-sea core off Portugal. Earth Planet Sci Lett, 249, 307-325, 2006.

Rousseau, D.D., Kukla, G., McManus, J.: What is what in the ice and the ocean? Quaternary Sci Rev, 25, 2025-2030, 2006.

K. L. Rosanski, Araguas-Araguas, R. Gonfiantini, in *Climate Change in Continental Isotopic Records*, P. K. Swart, K. C. Lohmann, J. McKenzie, S. Savin, Eds. (American Geophysical Union, Washington, DC), pp. 1–36, 1993.

Saltzman, Matthew & Thomas, E. (2012). Carbon Isotope Stratigraphy. The Geologic Time Scale, 1, 207-232. 2012.

Sánchez Goñi, M.F., Turon, J.L., Eynaud, F., Gendreau, S., European climatic response to millennial-scale changes in the atmosphere-ocean system during the Last Glacial Period. Quaternary Res, 54, 394-403, 2000.

Sánchez Goñi, M.F., Cacho, I., Turon, J-L., Guiot, J., Sierro, F.J., Peypouquet, J.-P., Grimalt, J.O., Shackleton, N.J.: Synchroneity between marine and terrestrial responses to millennial scale climatic variability during the last glacial period in the Mediterranean region. Clim Dynam, 19, 95-105, 2002.

Sánchez Goñi, M.F., Landais, A., Fletcher, W.J., Naughton, F., Desprat, S., Duprat, J.: Contrasting impacts of Dansgaard-Oeschger events over a western European latitudinal transect modulated by orbital precession. Quaternary Sci Rev, 27, 1136-1151, 2008.

Sánchez Goñi, M.F., Bard, E., Landais, A., Rossignol, L., d'Errico, F.: Air-sea temperature decoupling in western Europe during the last interglacial-glacial transition. Nat Geosci, 6, 837-841, 2013.

Sánchez Goñi, M.F., Rodrigues, T., Hodell, D.A., Polanco-Martinez, J.M., Alonso-Garcia, M., Hernandez-Almeida, I., Desprat, S., Ferretti, P.: Tropically-driven climate shifts in southwestern Europe during MIS 19, a low eccentricity interglacial. Geophys Res Abst, 18, EGU2016-3940, 2016.

889 Schneider, U., Becker, A., Finger, P., Meyer-Christoffer, A., Ziese, M., Rudolf, B.: GPCC's new
890 land surface precipitation climatology based on quality-controlled in situ data and its role in
891 quantifying the global water cycle. Theoret Appl Climatol, 115, 15-40, 2013.
892 Schneider, U., A. Becker, P. Finger, A. Meyer-Christoffer, M. Ziese, and B. Rudolf (2014),
893 GPCC's new land surface precipitation climatology based on quality-controlled in situ data
894 and its role in quantifying the global water cycle, Theor. Appl. Climatol., 115, 1–15.
895 Schrag, D.P, Hampt, G., and Murray, D.W.: Pore fluid constraints on the temperature and
896 oxygen isotopic composition of the glacial ocean. Science, 272, 5270, 1930-1932, 1996.
897 Spötl, C., Mangini, A., Richards, D.A.: Chronology and paleoenvironment of Marine Isotope
898 Stage 3 from two high-elevation speleothems, Austrian Alps. Quaternary Sci Rev, 25, 1127-
899 1136, 2006.
900 Stoll, H.M., Moreno, A., Mendez-Vincente, A., Gonzalez-Lemos, S., Jimenez-Sánchez, M.,
901 Dominguez-Cuesta, M.J., Edwards, R.L., Cheng, H., Wang, X.: Paleoclimate and growth
902 rates of speleothems in the northwestern Iberian Peninsula over the last two glacial cycles.
903 Quaternary Res, 80, 284-290, 2013.
904 Thatcher, D.L., Wanamaker, A.D., Jr., Denniston, R.F., Asmerom, Y., Ummenhofer, C.C.,
905 Polyak, V.J., Hasiuk, F., Haws, J.A., and Gillikin, D.P.: Changes in hydroclimate in Iberia in
906 the last 1200 years: insights from speleothem records from western Portugal. Geological
907 Society of America North-Central Meeting Abstracts with Programs, Ames, Iowa, 2018.
908 Trigo, R.M., Osborn, T.J., Corte-Real, J.M.: The North Atlantic Oscillation influence on Europe:
909 climate impacts and associated physical mechanisms, Clim Res, 20, 9-17, 2002.
910 Trouet, V., Esper, J., Graham, N.E., Baker, A., Scourse, J.D., Grank, D.C.: Persistent positive
911 North Atlantic Oscillation mode dominated the Medieval Climate Anomaly. Science, 324,
912 78-80, 2009.
913 Tzedakis, P.C., Roucoux, K.H., de Abreu, L., Shackleton, N.J.: The duration of forest stages in
914 southern Europe and interglacial climate variability, Science, 306, 2231-2235, 2004.
915 Vaks, A., Gutareva, O.S., Breitenbach, S.F.M., Avirmed, E., Mason, A.J., Thomas, A.L., Osinev,
916 A.V., Kononov, A.M., Henderson, G.M.: Speleothems reveal 500,000-year history of
917 Siberian permafrost. Science, 340, 183-186, 2013.
918 Vandenberghe, J., French, H.M., Gorbunov, A., Marchenko, S., Velichko, A.A., Jin, H., Cui,
919 Z., Zhang, T.,Wan, X.: The Last Permafrost Maximum (LPM) map of the Northern

Hemisphere: permafrost extent and mean annual air temperatures, 25-17 ka BP, Boreas, 43, 652–666, 2014.

Vegas, J., Ruiz-Zapata, B., Ortiz, J.E., Galan, L., Torres, T., Garcia-Cortes, A., Gil-Garcia, M.J., Perez-Gonzalez, A., Gallardo-Millan, J.L.: Identification of arid phases during the last 50 cal. ka BP from the Fuentillejo maar-lacustrine record (Campo de Calatrava Volcanic Field, Spain), J Quaternary Sci, 25, 1051-1062, 2010.

Voelker, A.H. L., Rodrigues, T., Stein, R., Hefter, J., Billups, K., Oppo, D., McManus, J,, Grimalt, J.O.: Variations in mid-latitude North Atlantic surface water properties during the mid-Brunhes (MIS 9-14) and their implications for thermohaline circulation, Clim Past, 6, p. 531-552, 2010.

Voelker, A.H.L. and de Abreu, L.: A review of abrupt climate change events in the northeastern Atlantic Ocean (Iberian Margin): Latitudinal, Longitudinal, and Vertical Gradients. Abrupt Climate Change: Mechanisms, Patterns, and Impacts (Eds. Rashid, H., Polyak, L., and Mosley-Thompson, E.), Geophysical Monograph Series 193, 15-37, 2011.

Wainer, K., Genty, D., Blamart, D., Daëron, M., Bar-Matthews, M., Vonhof, H., Dublyansky, Y., Pons-Branchu, E., Thomas, L., van Calsteren, P., Quinif, Y., and Caillon, N.: Speleothem record of the last 180 ka in Villars cave (SW France): Investigation of a large $\delta^{18}O$ shift between MIS6 and MIS5. Quaternary Sci. Rev., 30, 130-146, 2011.

Wassenburg, J.A., Immenhauser, A., Richter, D.K., Niedermayr, A., Riechelmann, S., Fietzke, J., Scholz, D., Jochum, K.P., Fohlmeister, J., Schröder-Ritzrau, Sabaoui, A., Riechelmann, D.F.C., Schneider, L., Esper, J.: Moroccan speleothem and tree ring records suggest a variable positive state of the North Atlantic Oscillation during the Medieval Warm Period. Earth Planet. Sci. Lett., 375, 291-302, 2013.

Zhou, J., Lundstrom, C.C., Fouke, B., Panno, S., Hackley, K., and Curry, B. Geochemistry of speleothem records from southern Illinois: Development of (^{234}U)/(^{238}U) as a proxy for paleoprecipitation. Chemical Geology, 221, 1-20, 2005.

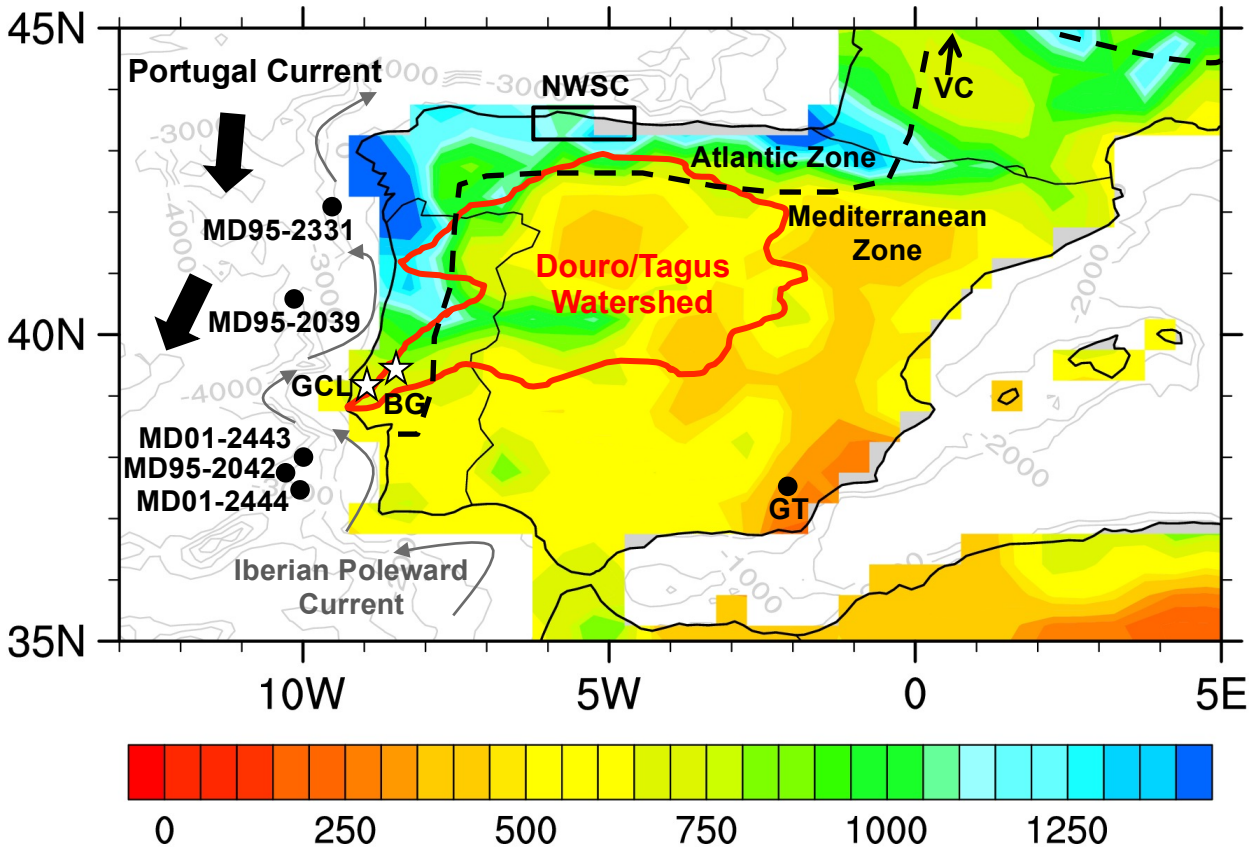

Figure 1. Average annual precipitation (mm) of the Iberian Peninsula for years AD 1901-2009 (GPCC v. 6; Schneider et al., 2013) relative to cave study sites (white stars: GLC = Gruta do Casal da Lebre; BG = Buraca Gloriosa). Rectangle denotes location of northwest Spain cave sites (NWSC) (Moreno et al., 2010; Stoll et al., 2013); FM = Fuentillejo maar (Vegas et al., 2010) and GT = Gitana cave (Hodge et al., 2008); VC = Villars Cave (Genty et al., 2003) located just north of map. Also shown are locations of marine cores discussed in text and GNIP stations at Porto, Vila Real, and Portalegre. Bathymetric contours shown in grey (m). Location of currents after Voelker et al. (2010).

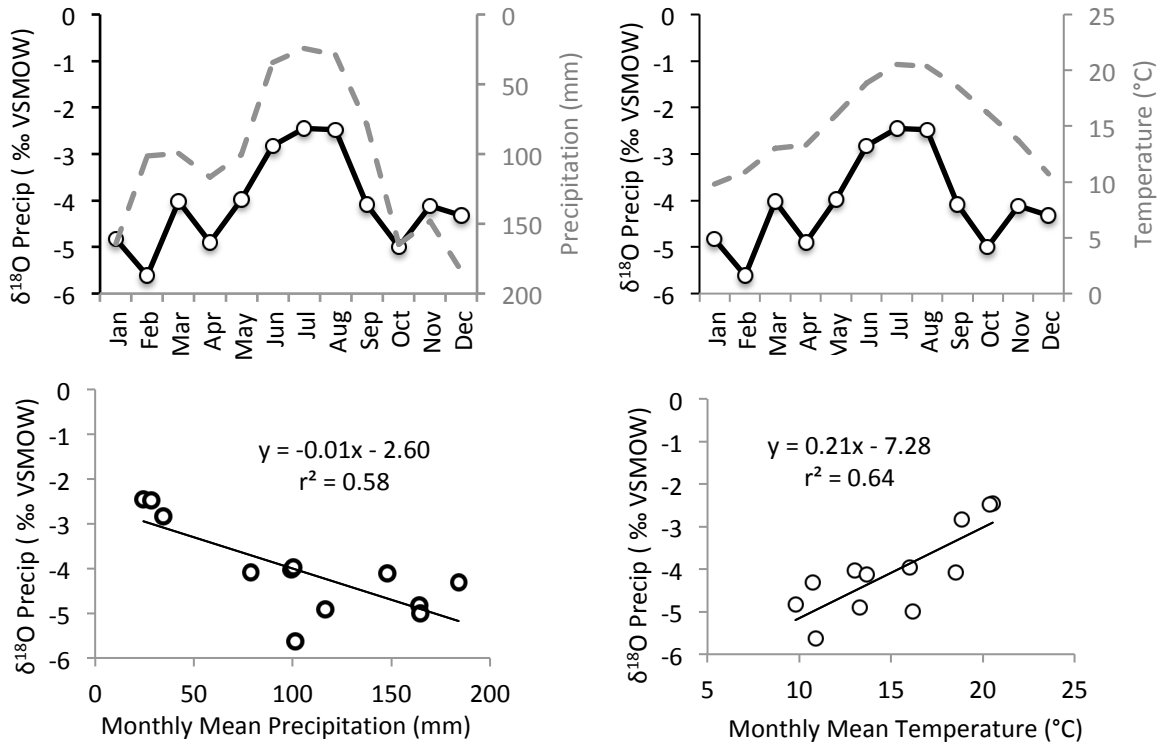

961
962
963

964 **Figure 2. Oxygen isotopic composition of precipitation versus rainfall amount (lefthand**
965 **panels) and air temperature (righthand panels).** Data collected at IAEA/GNIP site in Porto,
966 Portugal (see Fig. 1 for location) for 1988-2004. Oxygen isotope data represent multi-year
967 averages of monthly means. The two other closest GNIP stations in Portugal - Vila Real and
968 Portalegre (see Figure 1) - share similar relationships between precipitation oxygen isotopic
969 composition and air temperature (+0.27‰/˚C: r^2=0.76 and +0.26‰/˚C; r^2=0.69, respectively) to
970 that of Porto (+0.21‰/˚C). Note that right hand y-axis in upper left panel is inverted in order to
971 illustrate inverse nature of rainfall and precipitation oxygen isotopic composition.
972
973

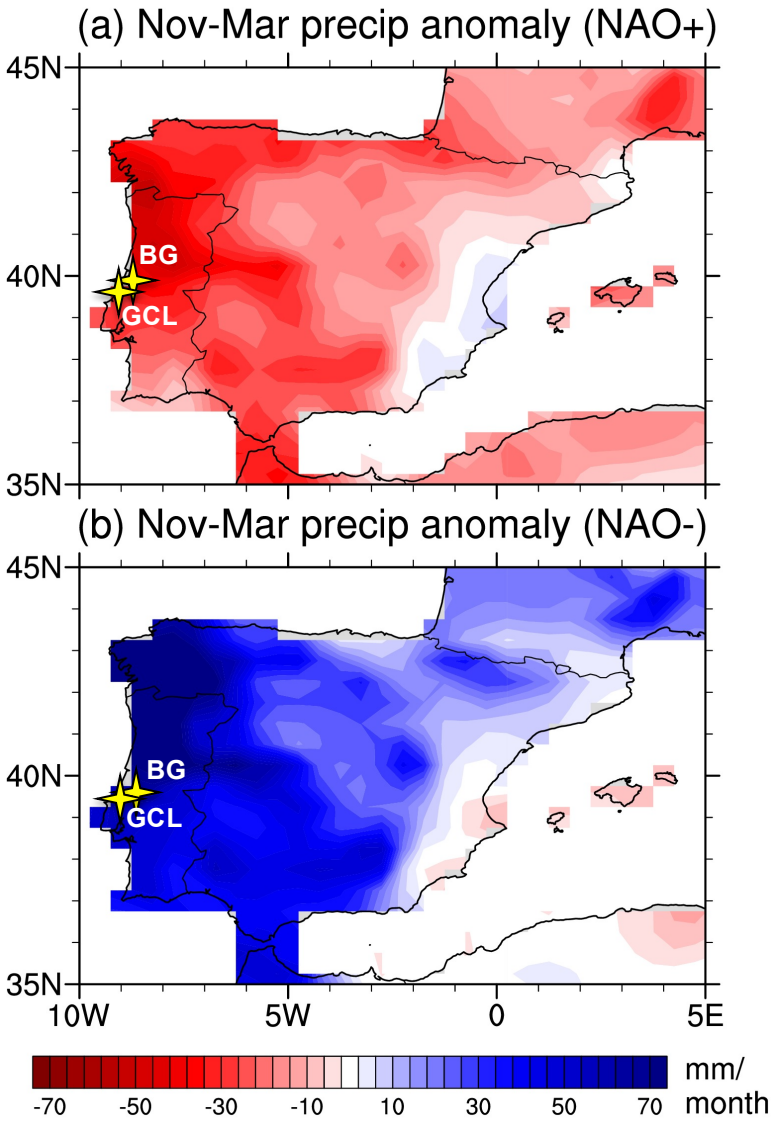

974

975 **Figure 3. Iberian rainfall anomalies associated with the North Atlantic Oscillation.**
976 Composites of November-March precipitation anomalies (mm/month) during (a) positive and (b)
977 negative NAO winters for the period 1901-2012. Positive/negative NAO winters were
978 determined using the December-March Hurrell principal component-based NAO index (CDG,
979 2018) as those winters with NAO values in the highest/lowest decile of all winters. The PC-
980 based NAO index represents the time series of the leading Empirical Orthogonal Function of
981 SLP anomalies over the Atlantic sector, 20°-80°N, 90°W-40°E. Precipitation anomalies are
982 based on the GPCC precipitation, version 7, at 0.5˚ spatial resolution (Schneider et al. 2014).
983 Yellow stars denote cave sites in this study: BG = Buraca Gloriosa; GCL = Gruta do Casal da
984 Lebre.

985

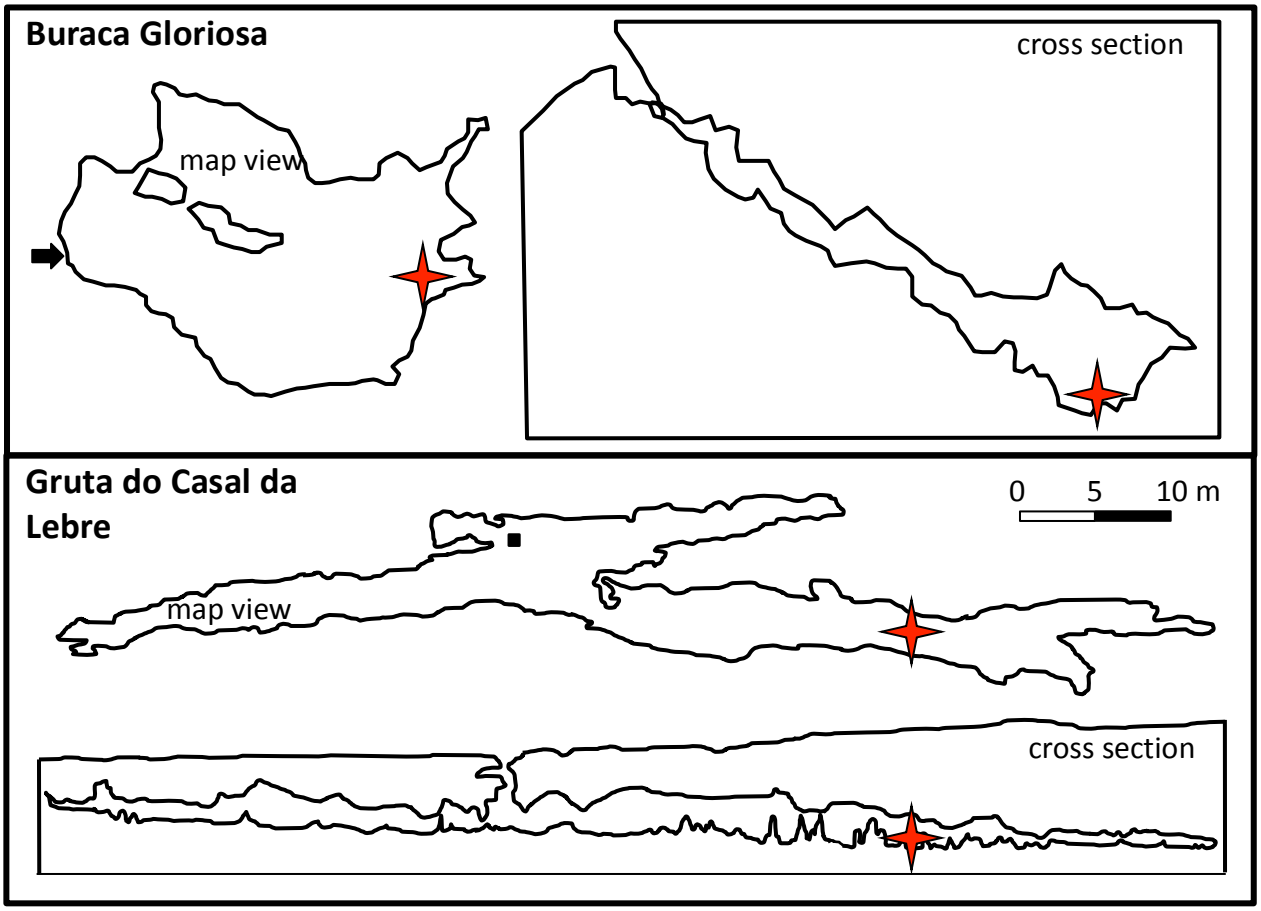

Figure 4. Profile and map views of Buraca Gloriosa (top) and Gruta do Casal da Lebre (bottom). Entrance denoted by arrow (top panel) and filled square (bottom panel). Red stars denote locations of stalagmites used in this study.

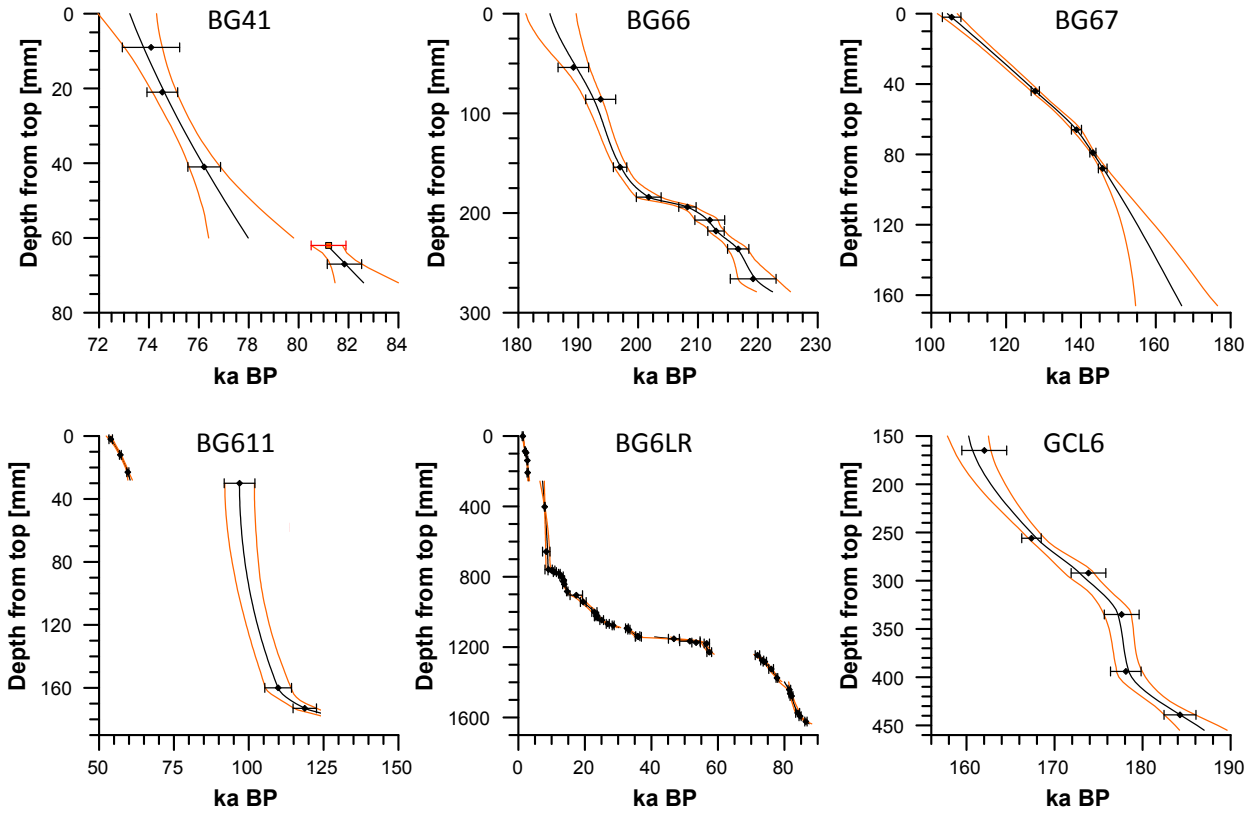

992

993 **Figure 5. COPRA-derived age models for BG/GCL stalagmites.** Black lines represent mean
994 of calculated age models while red lines denote 95% confidence intervals. See Table 1 for
995 specific ages and isotopic ratios. Orange square represents a "dummy age" that was included in
996 order to extrapolate below the hiatus, which is only possible with at least two dated points. The
997 bottom of BG611 was based on linear extrapolation through dated intervals. Distances for BG66
998 were measured relative to topmost section of interval for which stable isotopes were obtained,
999 and not relative to the cap of the stalagmite (see Figure 6).

1000

1001

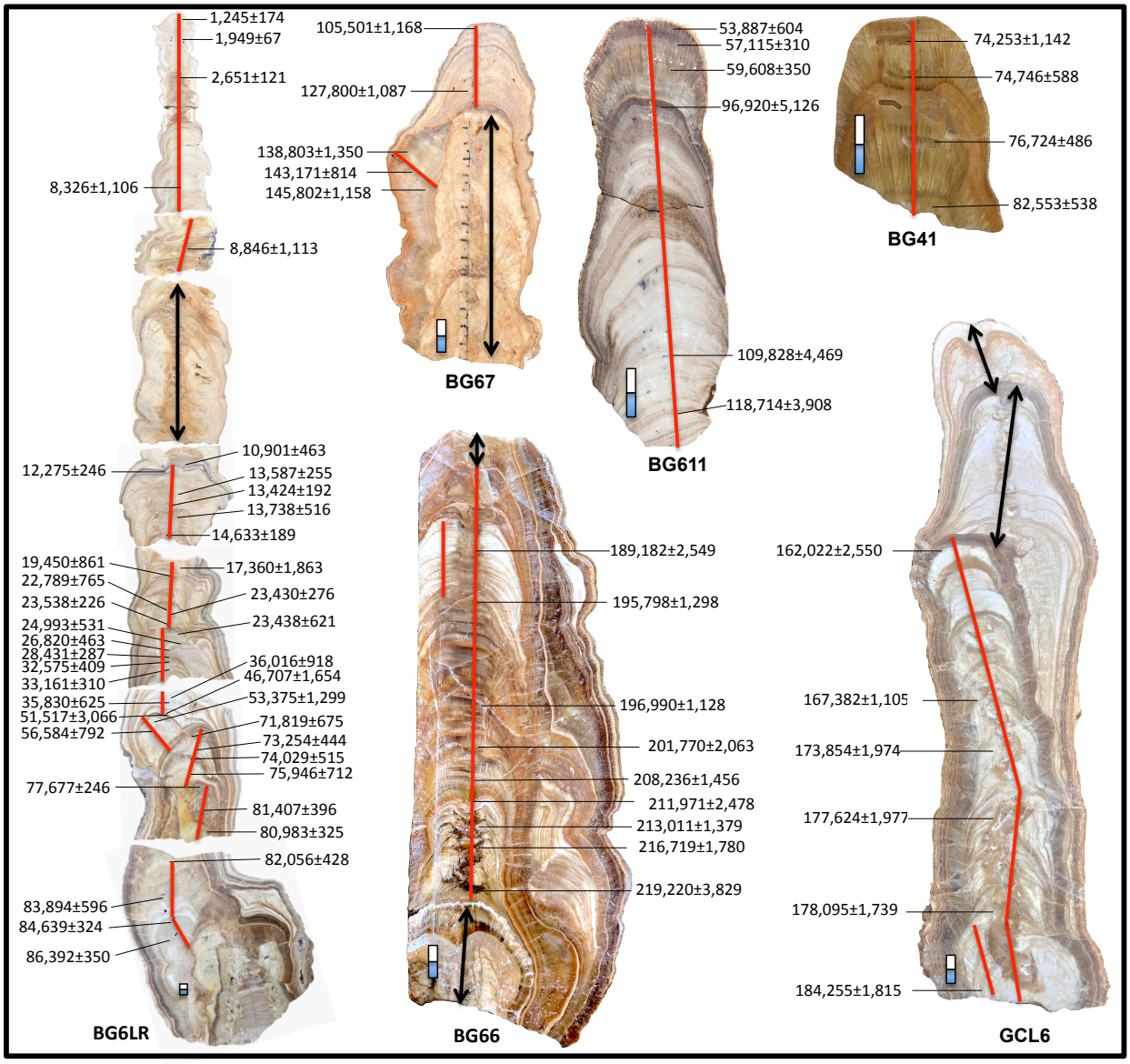

Figure 6. BG/GCL stalagmites and U/Th ages. Red lines denote stable isotope sampling transects. Blue and white scale bars (cm) define differential enlargement of each stalagmite. Black arrows represent intervals excluded from this study due to evidence of open system behavior. The impact of recrystallization in stalagmite cores was assessed by parallel sampling transects (parallel red lines on BG66 and GCL6) and demonstrated consistent stable isotopic values and trends (Supp. Fig. S7).

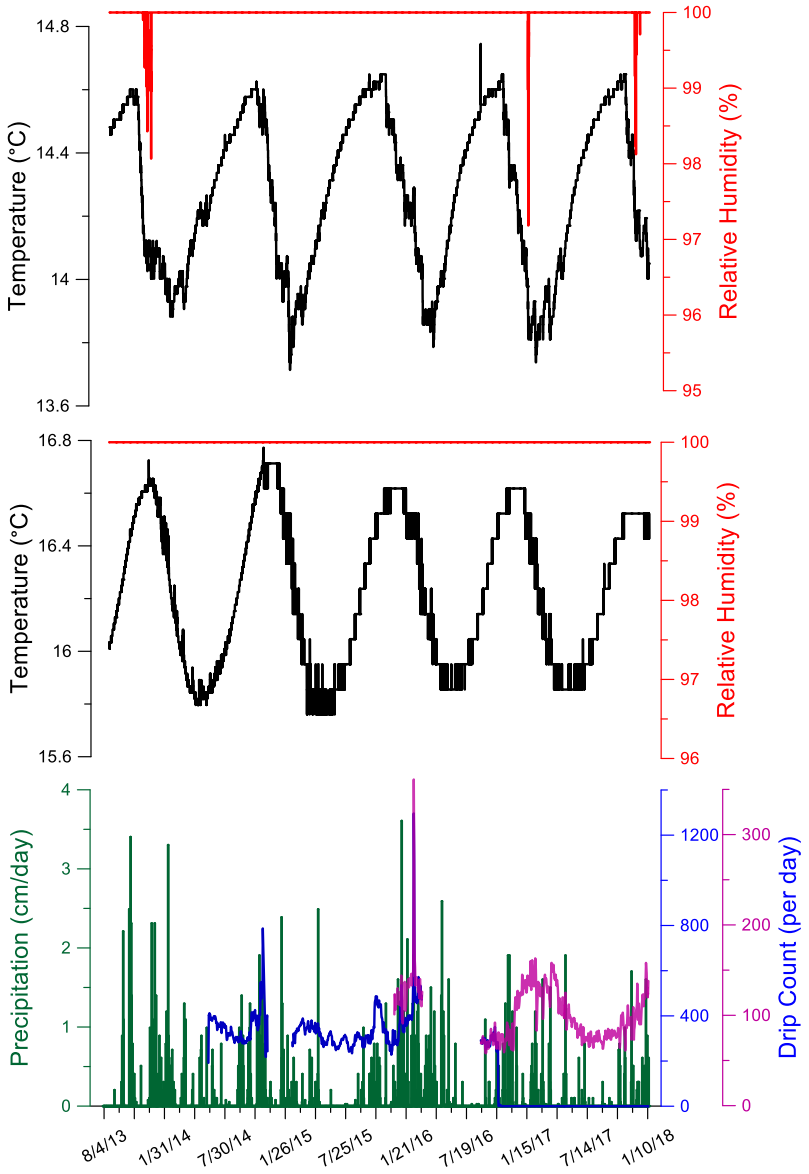

Figure 7. Temperature and relative humidity variations from (top) Buraca Gloriosa and (middle) GCL. Drip rate from Buraca Gloriosa and precipitation variability (bottom) from Monte Real, Portugal (35 km from BG). Temperature sensor in GCL was changed in November 2014 and the sensitivity of the new instrument varies slightly from the original.

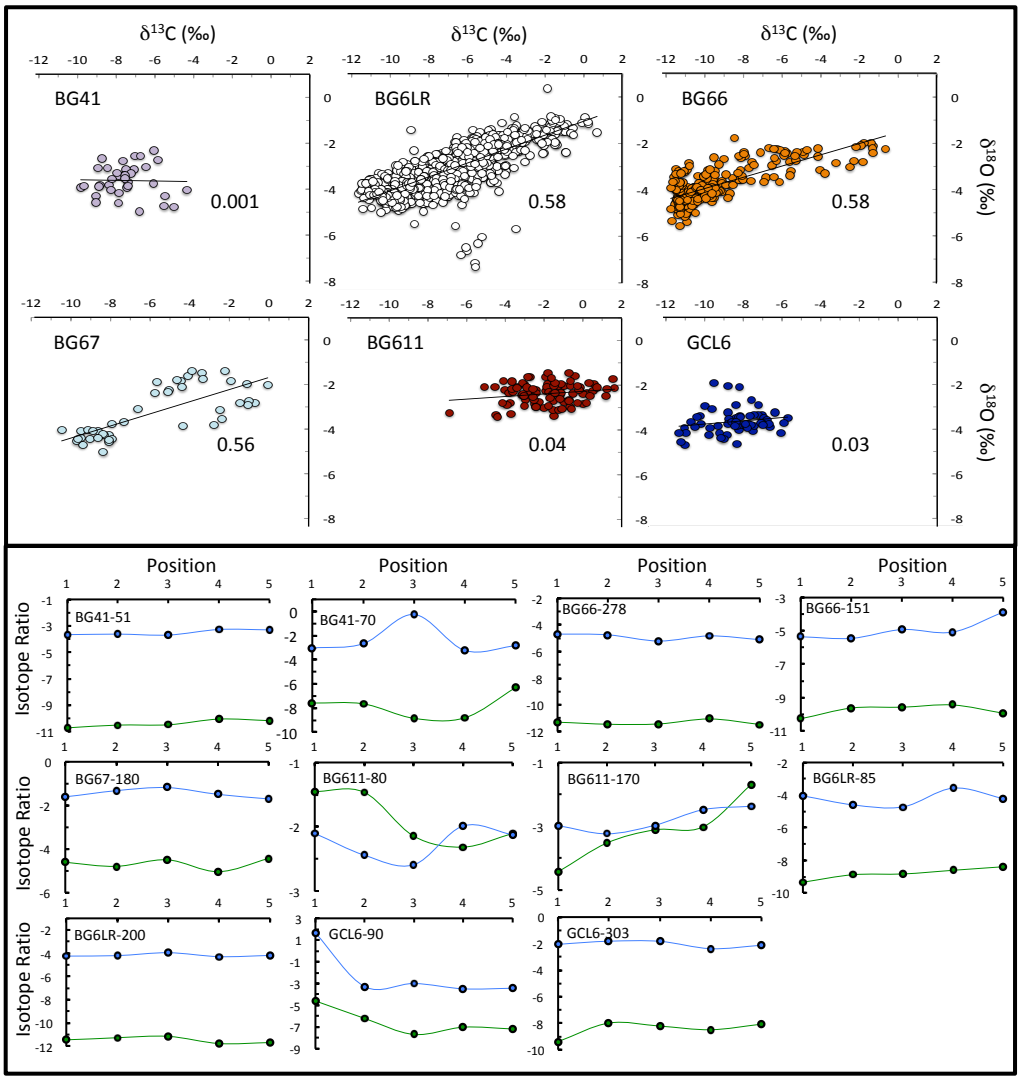

Figure 8. Hendy Tests of BG/GCL stalagmites. Top: Covariance plots of carbon and oxygen isotopic ratios. Correlation coefficients (r^2 values) are listed for each plot. High positive correlations have been identified as an indicator of non-equilibrium crystallization. Bottom: Oxygen (blue) and carbon (green) isotopic variations along the same growth layers with distance (listed in the upper left corner of each panel) from the stalagmite central growth axis. Progressive increases in $\delta^{18}O$ values have been interpreted to reflect disequilibrium crystallization. Limitations of the Hendy Tests are discussed in text.

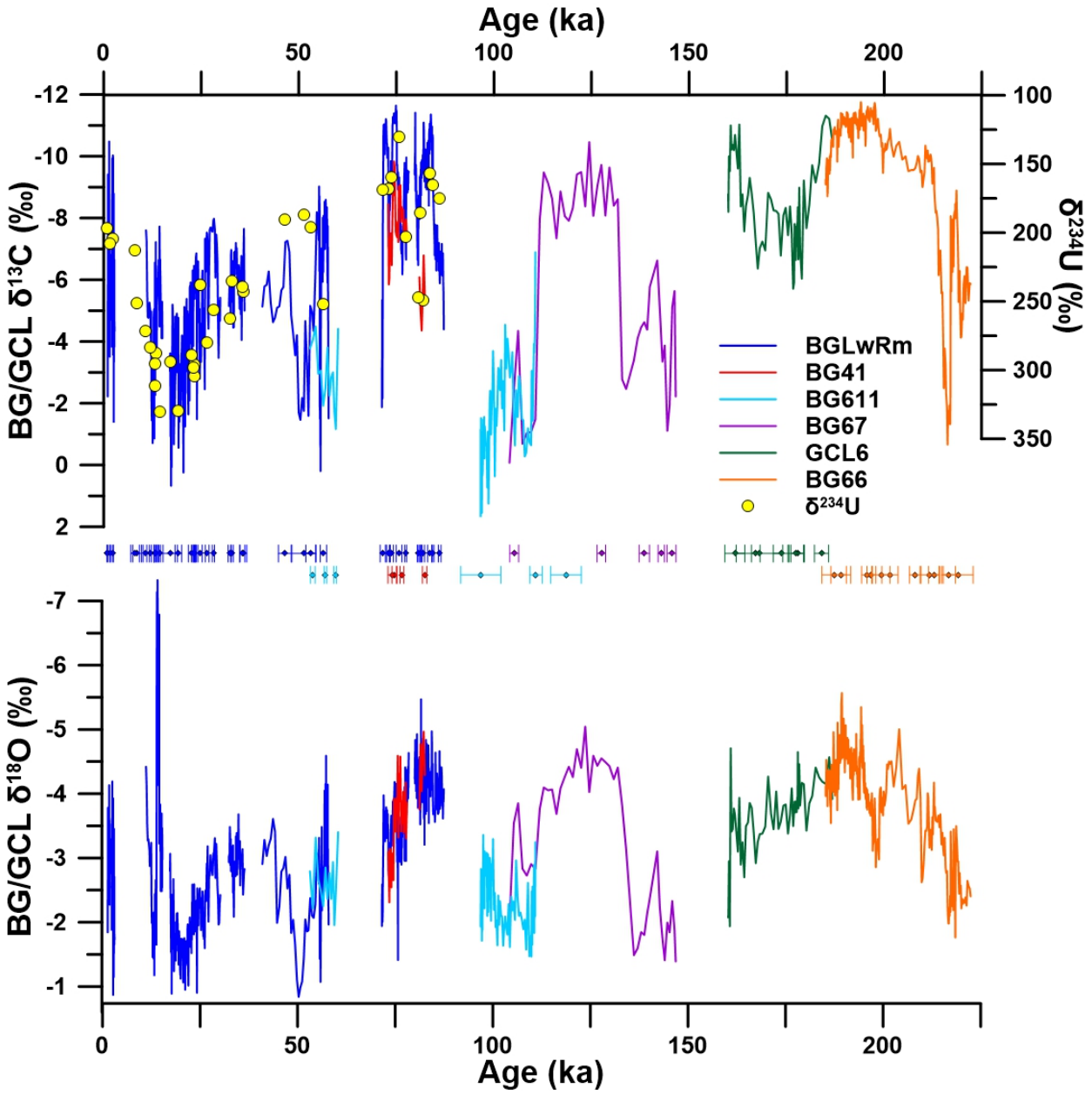

Figure 9. BG/GCL stalagmite isotopic time series. Carbon (top) and oxygen (bottom) isotopes, with each stalagmite presented in a different color. $\delta^{234}U$ values (yellow circles) for BG6LR are plotted against carbon isotope ratios (plots showing the $\delta^{234}U$ and $\delta^{13}C$ values of the other stalagmites are presented in the Supplemental Material). U/Th ages (with 2 s.d. errors) are also shown. The "?" at the MIS 6/5e transition denotes uncertainties associated with the continuity of this interval.

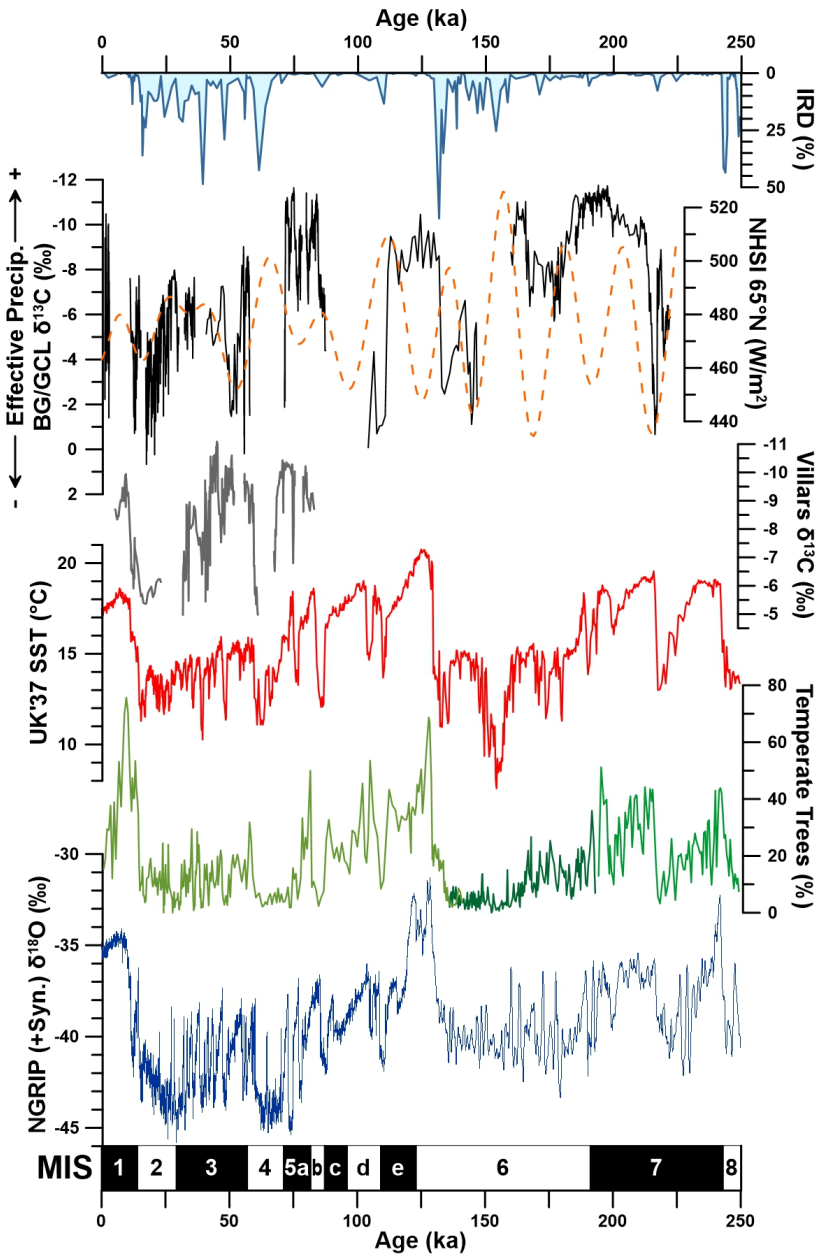

Figure 10. Comparison of Portuguese stalagmite hydroclimate proxies with regional and global climate records from the last two glacial cycles (A) Ice-rafted debris abundance from North Atlantic ODP Site 980 (McManus et al., 1999 using Hulu cave time scale as presented in Barker et al., 2011); (B) composite BG/GCL stalagmite carbon isotopic time series with NH summer insolation (Berger an Loutre, 1991); (C) Carbon isotopic time series from Villars Cave, southern France (Genty et al., 2003; Genty et al., 2006); (D) Alkenone-based Iberian margin SST reconstruction (core MD01-2443; Martrat et al., 2007); (E) Temperate forest pollen abundance from three closely spaced cores (MD01-2443: 250-194 ka (Roucoux et al, 2006; Tzedakis et al., 2004); MD01-2444: 194-136 ka (Margari et al., 2010; Margari et al., 2014); MD95-2042: 136-1 ka (Sánchez Goñi et al., 2008; Sánchez Goñi et al., 2013)); (F) NGRIP (0-122 ka) (North Greenland Ice Core Project members, 2004) and synthetic Greenland oxygen isotopic record (Barker et al., 2011) and (G) marine isotope stages.

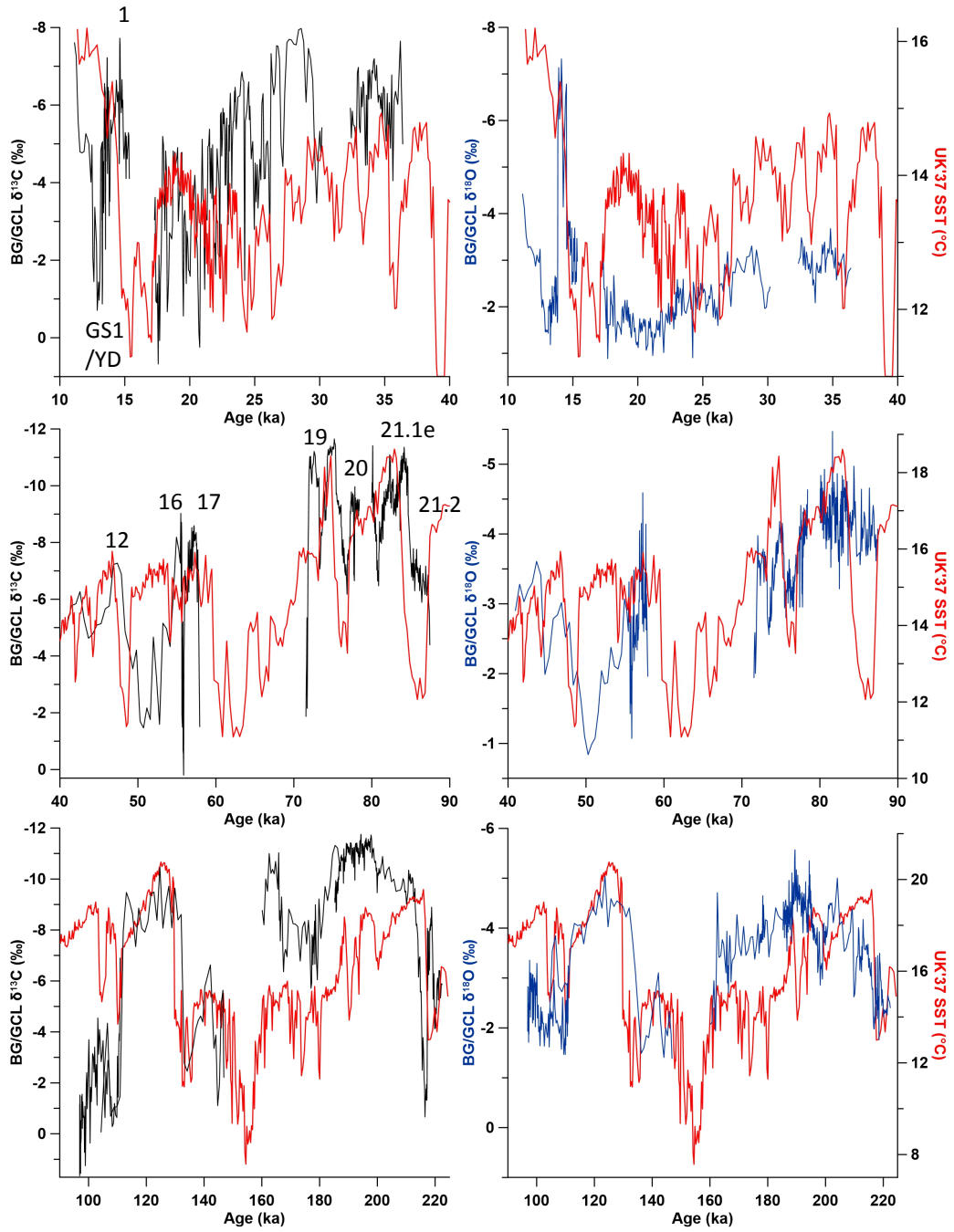

Figure 11. Iberian margin SST (red) and stalagmite carbon (black) and oxygen (blue) isotopes. Numbers denote select GI events using stratigraphic nomenclature of Rasmussen et al. (2014).

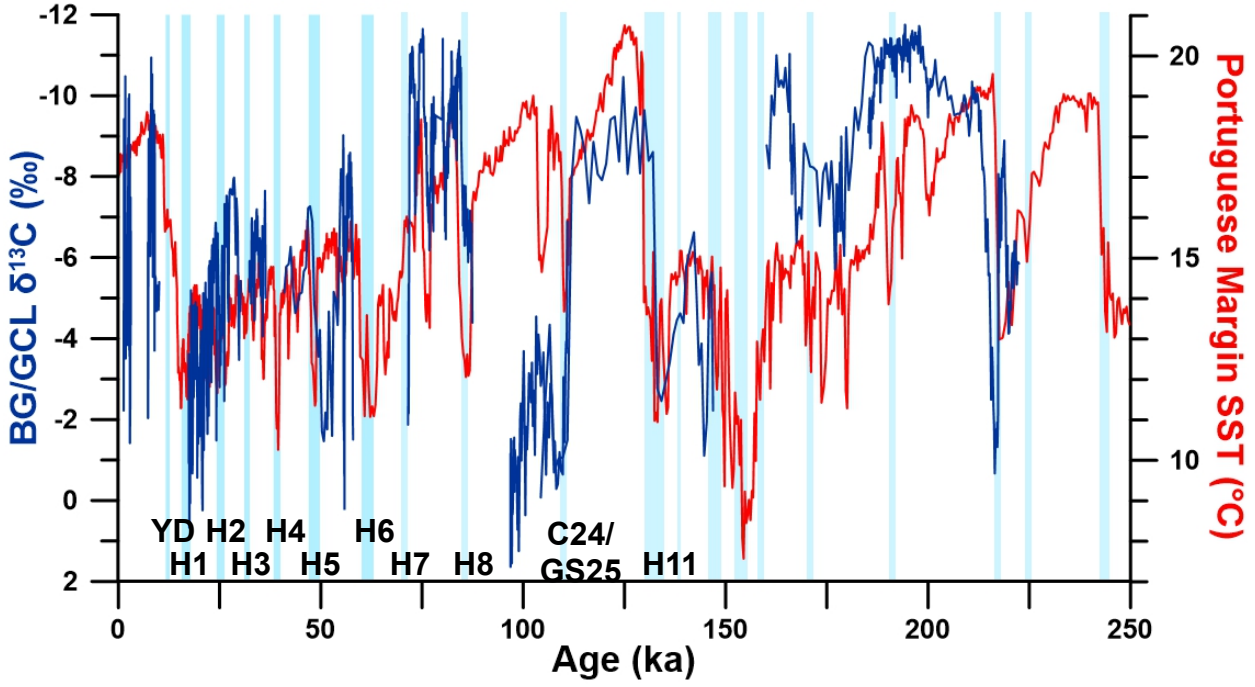

Figure 12. BG/GCL stalagmite carbon isotopic time series and Iberian margin SST. Light blue vertical rectangles denote North Atlantic cold events (some of which are labeled). Several interruptions in stalagmite growth coincide, within the errors of the stalagmite chronologies, with periods of depressed SST.

Table 1. U/Th Isotopic Ratios and ^{230}Th Ages

Stalagmite	Distance to Top (mm)	^{238}U (ng/g)	^{232}Th (pg/g)	δ^{234}U[a] (corr'd)	Error[b]	^{230}Th/^{238}U (activity)	Error	^{230}Th/^{232}Th (ppm)	Error	Uncorrected Age (yr BP)[c]	Error (yr)	Corrected Age (yr BP)[d]	Error (yr)
BG41	67	148	2,892	524.7	2.2	0.779	0.0023	657.7	18.6	82,926	389	82,553	538
BG41	41	293	4,635	522.8	2.2	0.742	0.0030	773.8	8.5	77,026	463	76,724	486
BG41	21	217	1,858	566.6	3.1	0.748	0.0039	1,440.0	40.6	74,906	567	74,746	588
BG41	9	271	2,088	610.8	9.8	0.764	0.0073	1,635.6	22.3	74,392	1,135	74,253	1,142
BG66	266	85	6,980	698.6	9.3	1.283	0.0057	256.5	1.8	223,637	3,252	219,220	3,829
BG66	236	123	4,742	520.6	4.1	1.169	0.0030	500.0	4.0	217,460	1,752	216,719	1,780
BG66	218	101	3,132	532.4	3.1	1.174	0.0015	623.6	4.6	214,835	1,052	213,011	1,379
BG66	207	75	4,657	429.2	3.8	1.116	0.0025	298.1	1.7	215,891	1,580	211,971	2,478
BG66	194	68	2,003	499.5	3.1	1.149	0.0019	644.2	7.4	210,002	1,175	208,236	1,456
BG66	184	95	4,336	379.4	3.1	1.073	0.0025	386.6	3.6	204,768	1,460	201,770	2,063
BG66	154	104	2,193	443.5	2.6	1.100	0.0015	864.2	11.9	198,297	930	196,990	1,128
BG66	86	104	2,661	345.4	2.4	1.041	0.0016	672.5	8.4	197,507	994	195,798	1,298
BG66	54	76	995	564.2	6.2	1.159	0.0057	1,453.3	64.3	189,936	2,538	189,182	2,549
BG67	88	320	2,153	617.8	2.9	1.095	0.0043	2,689.7	51.5	146,174	1,146	145,802	1,158
BG67	79	195	2,799	485.8	2.3	1.014	0.0022	1,164.3	18.2	144,037	695	143,171	814
BG67	66	250	4,187	610.3	4.9	1.072	0.0046	1,057.4	12.7	139,735	1,279	138,803	1,350
BG67	44	162	4,858	484.7	2.4	0.969	0.0023	531.9	5.3	129,620	608	127,800	1,087
BG67	2	216	5,542	401.5	2.6	0.837	0.0039	538.0	5.1	107,150	843	105,501	1,168
BG611	173	119	11,744	202.6	3.5	0.801	0.0041	133.9	0.8	126,291	1,253	118,714	3,908
BG611	**160**	110	12,828	230.9	4.6	0.792	0.0044	112.1	0.7	118,672	1,277	109,828	4,469
BG611	30	122	16,801	251.3	5.0	0.762	0.0043	91.2	0.5	107,202	1,088	96,920	5,126
BG611	23	313	552	340.8	1.4	0.553	0.0024	5,168.2	353.7	59,726	345	59,608	350
BG611	12	248	2,233	356.2	1.6	0.547	0.0021	1,002.4	25.4	57,908	296	57,115	310
BG611	2	250	4,109	376.7	1.8	0.533	0.0021	535.0	5.9	54,959	284	53,887	604
BG6LR	1,623	72	133	175.0	1.5	0.631	0.0015	5,665.9	1,162	86,532	342	86,392	350
BG6LR	1,593	98	140	165.3	1.4	0.618	0.0014	7,166.0	1,764	84,748	318	84,639	324
BG6LR	1,574	74	905	156.6	1.6	0.615	0.0016	824.8	25.3	84,848	360	83,894	596
BG6LR	1478	159	26	249.2	1.8	0.645	0.0021	63,745.2	114,070	82,068	428	82,056	428
BG6LR	1464	166	1,138	246.8	1.5	0.641	0.0009	1,542.3	35.8	81,475	214	80,983	325
BG6LR	1442	162	77	185.4	1.4	0.634	0.6339	21,885.5	13,015	81,442	396	81,407	396
BG6LR	1375	112	220	202.9	1.5	0.602	0.6016	5,064.2	652.0	77,823	234	77,677	246
BG6LR	1324	120	1,908	130.2	1.4	0.566	0.5660	585.8	15.3	77,213	330	75,946	712
BG6LR	1283	132	1,019	159.5	2.0	0.566	0.5659	1,213.9	71.1	74,623	422	74,029	515
BG6LR	1276	105	353	167.8	2.1	0.564	0.5637	2,766.4	298.1	73,512	425	73,254	444
BG6LR	1246	83	1,232	168.7	1.4	0.561	0.5613	625.8	14.2	72,957	369	71,819	675
BG6LR	1179	62	1,114	252.0	2.6	0.507	0.5071	464.4	15.9	57,877	465	56,584	792
BG6LR	1174	77	2,544	196.0	2.2	0.474	0.4736	235.4	3.8	55,882	375	53,375	1,299
BG6LR	1166	5	367	187.1	2.6	0.482	0.4821	100.4	1.6	57,644	524	51,517	3,066
BG6LR	1153	81	3,460	190.7	2.2	0.433	0.4331	167.2	2.3	49,960	367	46,707	1,654
BG6LR	1141	52	1,159	242.6	2.8	0.359	0.3591	266.4	10.4	37,626	449	36,016	918
BG6LR	1138	55	750	239.5	1.8	0.352	0.3518	426.3	33.1	36,815	381	35,830	625
BG6LR	1101	71	283	235.2	2.0	0.323	0.3234	1,344.2	198.7	33,449	272	33,161	310
BG6LR	1093	70	472	262.1	2.1	0.327	0.3269	802.0	73.4	33,052	331	32,575	409
BG6LR	1077	101	595	256.6	1.8	0.290	0.2899	810.6	63.4	28,851	193	28,431	287
BG6LR	1068	85	1,034	280.0	1.4	0.285	0.2847	384.9	15.5	27,675	178	26,820	463
BG6LR	1046	56	705	238.2	2.2	0.260	0.2603	339.0	19.7	25,911	265	24,993	531
BG6LR	1026	123	2,093	304.1	1.9	0.262	0.2617	253.3	8.5	24,612	206	23,438	621
BG6LR	1025	123	493	296.4	1.4	0.253	0.0017	1,041.2	151.0	23,814	175	23,538	226
BG6LR	1019	80	377	298.5	2.1	0.252	0.2525	887.3	107.4	23,753	221	23,430	276
BG6LR	1001	68	1,464	288.7	1.5	0.256	0.2558	196.1	4.3	24,291	156	22,789	765
BG6LR	944	76	1,896	329.3	2.1	0.233	0.2330	154.8	3.9	21,131	196	19,450	861
BG6LR	899	79	4,209	294.0	3.4	0.227	0.2266	70.6	1.3	21,074	283	17,360	1,863
BG6LR	883	91	233	330.3	2.0	0.168	0.1684	1,082.0	213.7	14,806	165	14,633	189
BG6LR	843	100	1,409	287.7	4.0	0.162	0.1623	190.4	6.7	14,718	164	13,738	516
BG6LR	827	103	332	295.0	2.9	0.152	0.1521	783.5	116.9	13,645	154	13,424	192
BG6LR	819	75	491	311.6	1.4	0.158	0.1581	400.0	22.8	14,032	123	13,587	255
BG6LR	783	95	525	283.8	2.2	0.141	0.1406	418.7	35.3	12,661	150	12,275	246
BG6LR	774	107	1,351	271.4	1.4	0.130	0.1304	169.8	5.7	11,795	119	10,901	463
BG6LR	759	135	4,177	251.5	1.5	0.121	0.1210	64.7	1.0	11,071	117	8,846	1,113
BG6LR	657	86	2,566	212.9	1.4	0.112	0.1120	62.1	0.9	10,540	96	8,326	1,106
BG6LR	139	172	323	204.2	1.7	0.031	0.0010	272.6	41.0	2,790	96	2,651	121
BG6LR	86	155	80	207.9	1.7	0.022	0.0007	720.9	312.3	1,987	62	1,949	67
BG6LR	10	122	43	196.7	18.9	0.014	0.0019	677.5	519.3	1,271	173	1,245	174
GCL6	439	91	2,815	76.3	2.3	0.862	0.0029	461.2	9.3	185,093	1,779	184,255	1,815
GCL6	394	86	3,009	125.7	2.0	0.881	0.0032	415.9	6.9	179,002	1,692	178,095	1,739
GCL6	335	70	4,579	82.7	3.0	0.856	0.0029	214.9	2.3	179,406	1,794	177,624	1,977
GCL6	292	75	2,61	78.2	2.9	0.845	0.0035	481.0	9.0	174,639	1,949	173,854	1,974
GCL6	256	116	1,019	86.2	2.2	0.836	0.0020	1,574.3	71.8	167,617	1,102	167,382	1,105
GCL6	165	94	2,507	122.4	4.2	0.847	0.0049	526.3	13.4	162,712	2,368	162,022	2,550

[a] $\delta^{234}U_{meas'd} = [(^{234}U/^{238}U)_{meas'd}/(^{234}U/^{238}U)_{eq}-1] \times 10^3$, where $(^{234}U/^{238}U)_{eq}$ is secular equilibrium activity ratio: $\lambda_{238}/\lambda_{234} = 1.0$. Values reported as permil.

[b] Errors are at the 2σ level.

[c] Present is defined as the vear AD 1950.

[d] Initial ^{230}Th/^{232}Th atomic ratio of $13.5\times10^{-6} \pm 6.75\times10^{-6}$ used to correct for unsupported ^{230}Th in BG stalagmites. GCL stalagmites use $4.4\times10^{-6} \pm 2.2\times10^{-6}$.

1069